NUMERICAL MODELLING OF THE PROPAGATION ENVIRONMENT IN THE ATMOSPHERIC BOUNDARY LAYER OF LITTORAL AREAS

Horizontal Variations in the Marine Boundary Layer

R. S. Plant and B. W. Atkinson

Department of Geography
Queen Mary and Westfield College
University of London

Phase 2 - Report No 2
MoD Agreement No. FS2/2042/02

January 2000

Contents

Abstract

Phase 1 of this project was successful in simulating many features of the propagation environment, in agreement with aircraft observations. A marine internal boundary layer (MIBL), of realistic depth, resulted from the flow of hot, dry air from Saudi Arabia over the Persian Gulf. The simulations also generated a sea-breeze circulation. Although this was located outside the observation region, its existence is supported by general arguments, including many observations that have been made under similar conditions. However, the simulations run for phase 1 were not able to detect any of the short–scale (10 to 20 km) horizontal variations in the mature marine boundary layer (MBL) that were found in the aircraft observations.

The phase 1 simulations used 33 vertical levels and a horizontal grid length of 6 km. In the present report, the numerical resolution has been enhanced in an attempt to capture short–scale variations. Taking 41 vertical levels and a 1 km horizontal grid length, there was no evidence for such variations in the mature MBL. The observed short–scale variations can therefore not be explained with the mesoscale model as it stands.

The enhanced resolution has revealed some unusual perturbations in the developing MIBL, which have a significant effect on the refractivity environment within $\sim$ 100 km of the coast. We believe that the perturbations are genuine and observable phenomena, which have a simple physical interpretation. They are caused by the presence of the strong sea-breeze circulation, which modifies the MIBL growth mechanism. In the low wind case, the MIBL just out to sea is very moist, due to the on-shore flow of the sea breeze which transports marine air towards the coast. In the high wind case, there is little onshore flow, but the sea-breeze circulation strongly retards the prevailing offshore wind. For a fixed distance travelled the retarded air has additional time in which to respond to the change in surface conditions. This can lead to an extremely rapid deepening of the MIBL. Our interpretations are based on qualitative arguments, a detailed analysis of the simulation results and a generalization of an established MIBL analytic model.

1 Introduction

This project is concerned with assessing the capability of mesoscale numerical models for predicting the propagation environment in coastal areas. Phase 1 covered the testing of a non-hydrostatic, numerical model in idealised and realistic situations (Li and Atkinson, 1997a; Li and Atkinson, 1997b; Li and Atkinson, 1998a; Li and Atkinson, 1998b). The realistic cases (Li and Atkinson, 1998b) were run to simulate conditions in the Persian Gulf in a period when aircraft observations had been taken (Brooks *et al.*, 1997; Brooks *et al.*, 1999). The results were encouraging and showed that the model was capable of capturing the essential features of the propagation environment. A marine boundary layer (MBL) over the Gulf was well simulated in both its depth and the gradients of temperature, humidity and refractivity therein. In addition to the important vertical gradients at the top of the MBL, well-developed sea-breeze circulations were found which exhibited a strong horizontal gradient at the boundary between sea and land air. It is tempting to call this gradient the sea-breeze front (SBF), but care in nomenclature is required here as observations of such fronts show them to be hundreds of metres, rather than several kilometres, wide.

In the light of the results from Phase 1 it was decided to pursue four aspects of the project: first, the effects of horizontal grid resolution on the simulations; second, a more detailed analysis of the SBF; third, horizontal variations within the MBL; fourth, the incorporation of the TERPEM model, a code that allows calculation of the response of electromagnetic radiation to the propagation environment produced by the meteorological model. The effects of grid resolution have been discussed by Plant and Atkinson (1999). This report covers horizontal variations.

2 Horizontal Variations

Atmospheric conditions within the planetary boundary layer are controlled by properties of the underlying surface. If air flows over a point where there is a discontinuity in the surface properties, it will have to adjust itself to the prevailing situation. In the present case, air flows from the hot, dry desert of Saudi Arabia over the Persian Gulf. The air can respond more quickly to the change the closer it is to the surface and so an internal boundary layer (IBL) develops (Garratt, 1990), deepening as the exposure to sea-surface conditions increases. Eventually, an equilibrium height is attained where the atmosphere has become well-adjusted and is characteristic of marine conditions. The aircraft observations reported by Brooks *et al.* (1997; 1999) were taken within such a well-adjusted region — any overall trends that

were discernible within the observation region appear to have been modest[1]. Interestingly, however, the observations revealed significant variation in the boundary layer duct depth (see Table 3 of Brooks *et al.* (1999)). Similarly, Brooks *et al.* (1997) stated that "there is no general trend in BL height, but ... there is considerable variability on a scale of 10 to 20 km". It was even tentatively suggested that "the variation looks wavelike in nature" although the sampling frequency seems to have been insufficient for gravity waves to have been explicitly resolved.

Although many features of the observations made by Brooks *et al.* have been successfully captured in the modelling studies (Li and Atkinson, 1998b; Atkinson and Li, 1999; Plant and Atkinson, 1999), no evidence for significant small–scale horizontal variability has been found. This is despite the fact that horizontal grid lengths used in the mesoscale numerical model were reduced as far as 3 km by Plant and Atkinson (1999), which will have allowed for several grid points to have been positioned within the reported length scale of the variations. For the present report, the numerical resolution has been further increased in an attempt to capture the variations. However, no such behaviour has been identified, even with horizontal and vertical grid point separations of 1 km and 10 m respectively. (Some example cross sections of refractivity from this high–resolution model run, along horizontal lines in the domain, can be seen in Fig. 1.) Additional improvements to the numerical resolution do not appear to be justified and would require prohibitive amounts of computing time. Thus, it seems reasonable to conclude that an explanation for the observed short–scale horizontal variations requires either significantly–improved input data or the incorporation of new physics into the current mesoscale model.

For example, a defect of the model that was pointed out by Li and Atkinson (1998b) may prove to be relevant. A fixed sea-surface temperature is used, which depends neither on time nor position. Variations in the sea-surface temperature may not obviously be of great import, but they nevertheless provide an attractive candidate mechanism by virtue of introducing some natural element of inhomogeneity into the well-adjusted, slowly–varying system. Moreover, it is interesting to note the remark by Brooks *et al.* (1999) that "All of the regions of increased duct depth are associated with regions of decreased sea–air temperature difference."

[1] A moistening of the boundary layer downwind was noted by Brooks *et al.* (1997; 1999). However, an increase by 1.2 g/kg along the entire flight path (Brooks *et al.*, 1997) is certainly not sufficient to explain short–scale horizontal variations.

3 Perturbations in the Marine Internal Boundary Layer

Plant and Atkinson (1999) found that grid lengths as coarse as 15 km could be used for qualitative studies of the propagation environment. However, the strong gradients associated with the marine internal boundary layer (MIBL) were more accurately captured at finer resolutions. The fine resolution runs were also able to reveal a perturbation in the MIBL in the 'low wind' case. This was noticed in contour plots of humidity and refractivity (Figs. 3a and 4a of Plant and Atkinson (1999)) and indicated that the near-surface marine air near the coast was unexpectedly moist. Further out to sea, there was surprisingly little change of humidity for a significant distance downstream, until a gradual moistening began again at a fetch of $\sim$ 100 km. This behaviour appeared to be related to the sea-breeze circulation since a SBF was located very near to the coast and onshore winds persisted roughly up to the point where moistening recommenced (Fig. 5a of Plant and Atkinson (1999)). Unfortunately, this behaviour could neither be confirmed nor denied from the aircraft observations, since no data were taken immediately downwind of the coast. Nonetheless, the perturbation does have a significant effect on the distribution of refractivity in the lowest few hundred metres of the atmosphere and represents a notable departure from the normal picture of MIBL structure (Garratt, 1990).

As detailed in Sec. 4, the mesoscale numerical model has been run with improved resolution for this report. An increase to the vertical resolution has brought out another MIBL perturbation, this time in the 'high wind' case. A very rapid deepening of the MIBL occurs about 50 km offshore, close to the position of the SBF.

In the remainder of this report, we investigate the origin and the structure of the simulated MIBL perturbations. After a brief description of the simulations (Sec. 4) and of the perturbation arising in the high wind case (Sec. 5), we discuss in some detail (Sec. 6) an existing MIBL analytic model due to Garratt (Garratt, 1987; Garratt and Ryan, 1989; Garratt, 1992). We then explain why this model fails in the present simulations (Sec. 7.2) and suggest a 'generalized Garratt model' in order to overcome its deficencies. Although requiring considerable input from the simulation results, the generalized model framework is very successful in accounting for the perturbation observed in the high wind case (Sec. 7.3). The manner in which the generalized model can incorporate the perturbation lends strong support to our more general arguments about the interaction between the sea-breeze circulation and the normal mechanism of MIBL development (Sec. 8). Sec. 9 discusses the perturbation found in the low wind case, and our conclusions are presented in Sec. 10.

4 Mesoscale Model Runs

Following the categorization of Brooks *et al.* (1997; 1999), simulations of the propagation environment in the Persian Gulf have been performed under both 'low' ($\sim$ 5 ms^{-1}) and 'high' ($\sim$ 15 ms^{-1}) wind conditions. Apart from some numerical aspects (detailed below), the mesoscale model runs performed for the purposes of the present report are identical to those of Plant and Atkinson (1999), who gave a general description of the modelling. Many aspects of the simulation results have been presented and discussed in earlier reports (Li and Atkinson, 1998b; Atkinson and Li, 1999; Plant and Atkinson, 1999).

In order that variations in the boundary layer might be more easily ascertained, the vertical resolution has been enhanced. A total of 41 vertical levels is used. Using the same initial profiles of humidity and potential temperature as Plant and Atkinson (1999), and setting a pressure field through the hydrostatic approximation (Li and Atkinson, 1997b), gave the initial conditions of Table 1.

Some numerical experiments were performed on the required extent of the horizontal grid. In previous work (Li and Atkinson, 1998b; Atkinson and Li, 1999; Plant and Atkinson, 1999) the model grid had dimensions of 600 by 360 km ($-300 \leq x \leq 300$ and $-180 \leq y \leq 180$). In the current set of runs, however, the model grid has been restricted to the area $-180 \leq x \leq 120$ km and $-120 \leq y \leq 0$ km, the origin of co-ordinates remaining unaltered. Neglecting effects close to the boundary of the new domain, the simulated results have been found to be in good agreement with those obtained on the original domain. The reason for cutting down the simulated area has been to reduce the computing time required by the numerical simulations. This has been necessary in order to render as practical the model run with a 1 km grid length. The coastline within the new domain is shown in Fig. 2.

Finally, we note a reduction to the time step used in the numerical model. In previous work, a time step of 20 s was found to be satisfactory. This choice produced an instability when using 41 vertical levels and a 3 km grid length, but a modest reduction to 15 s proved to be acceptable. The same time step could also be used successfully with a 1 km grid length, provided that the horizontal diffusion coefficients were reduced (the purpose of these coefficients within the model was described by Ballard and Golding (1991)). The momentum diffusion coefficient was changed from $15,000$ m^{2}s^{-1} to $10,000$ m^{2}s^{-1} and the heat coefficient from $7,500$ m^{2}s^{-1} to $5,000$ m^{2}s^{-1}.

In the following discussion of the simulated MIBL, we shall concentrate on results obtained along an east-west line in the model domain. The line is identical to that used for the comparison with aircraft observations (Brooks *et al.*, 1997; Brooks *et al.*, 1999) in previous reports from this project (Li and Atkinson, 1998b; Atkinson and Li, 1999; Plant and Atkinson, 1999). Unless

otherwise stated, the accompanying figures were produced from data along $y = -54$ km at 1500 hr in the high–wind run with a 3 km grid length. When examining the figures, the reader should bear in mind that the numerical grid co-ordinate x is in use throughout. The east-west line lies over the land surface from the western domain boundary up to $x = -99$ km and over the sea thereafter. Thus, to convert from x to a fetch, it is simply necessary to add 99 km. Some comments about results obtained at other times and places can be found in the more general discussion of Sec. 8.

5 Structure of the MIBL

Around fifteen years ago, the stable internal boundary layer had received relatively little attention. Analysis (Raynor *et al.*, 1975; Mulhearn, 1981; Hsu, 1983) had concentrated on establishing a pattern of growth or on obtaining an equilibrium value for the depth of the layer. Although limited to simple phenomenological and dimensional arguments, such work was nevertheless valuable, and often provided an important component in modelling and understanding the dispersal of coastal pollution. More recently, a programme of detailed aircraft observations enabled Garratt and Ryan (1989) to provide an improved description of the MIBL, backed up by the results from a mesoscale numerical model (Garratt, 1987). A series of assumptions that were suggested by the numerical experiments led Garratt (1987) to propose the following relation for MIBL growth:

$$h^2 = \alpha^2 U^2 \left(\frac{g \Delta\theta}{\overline{\theta}} \right)^{-1} x, \tag{1}$$

where:

- h is the IBL height (m);
- U is the ambient wind component perpendicular to the coast (ms^{-1});
- x is the fetch (km);
- $\Delta\theta$ is the potential temperature difference between the air over land and at the sea surface (K); and,
- $\overline{\theta}$ is an average potential temperature[2] for the IBL (K).

[2]This quantity is simply described as "the mean potential temperature" in the literature, which is somewhat ambiguous. For instance, it would seem reasonable to interpret the phrase as meaning the average of the potential temperatures over land and at the sea surface, the quantities used in defining $\Delta\theta$. The correct interpretation is quite clear from the origin of this factor in the derivation (see Sec. 6.5) and has $\overline{\theta} = \int_0^h \overline{w'\theta'} dz [\int_0^h \theta^{-1} \overline{w'\theta'} dz]^{-1}$. In practice, it is good enough to choose $\overline{\theta}$ to be a typical IBL potential temperature.

The dimensionless quantity α is predicted by the model, but in practice seems to be used as a quantity to be fit to the data (Garratt and Ryan, 1989; Hsu, 1989).

Owing to a perturbation in the simulated MIBL, the $h \sim \sqrt{x}$ growth of Eq. 1 (and of other suggested relations (Raynor *et al.*, 1975; Mulhearn, 1981; Hsu, 1983)) does not provide a good representation of the simulation results. This can be seen from Fig. 3, where the height of the MIBL is plotted along the line $y = -54$ km. A jump at $x \sim -50$ km is immediately obvious. (It must be stated here that the precise definition of a stable IBL height is open to debate, a variety of methods for determining the height having been suggested in the literature (a number of the possibilities are mentioned, for example, by Stull (1988)). Applications of various methods to the present situation are discussed in Appendix A. Throughout the main body of this report, we have chosen to use an approach which identifies the IBL height with the top of the inversion. This approach is referred to as 'method 3' in Appendix A, where its detailed implementation is described.) Note that the dip in the MIBL height that is seen for the last few grid points in Fig. 3 is a purely–artificial numerical boundary effect. Similar effects can also be seen in other plots derived from the simulation data.

Eq. 1 was originally derived by Garratt (1987). Shortly afterwards, however, it was pointed out (Garratt and Ryan, 1989) that some of the assumptions that were made by Garratt (1987) are unnecessary. A more general treatment has been described (Garratt and Ryan, 1989; Garratt, 1992), leading to the same final growth equation, but with a modified expression for α. It is interesting to test the validity of the assumptions made in the literature in order to find out how the model breaks down in the present case. For convenience, the model derivation is repeated below[3].

6 Garratt's IBL Growth Equation

The starting point for Garratt's model is the potential temperature equation[4],

$$\frac{D\theta}{Dt} = -\frac{1}{\rho}\frac{\partial}{\partial z}(\rho\overline{w'\theta'}) + R + F_\theta, \tag{2}$$

where R is a radiative term and F_θ represents horizontal diffusion. D/Dt denotes the advective derivative and all other symbols have their usual meaning

[3]We also wish to clarify the model, since the published derivations (Garratt, 1987; Garratt and Ryan, 1989; Garratt, 1992) differ somewhat from each other and contain some minor errors.

[4]Garratt (1992) works in terms of the virtual potential temperature instead. It has been found through explicit calculation, however, that this has very little effect on the results obtained by applying a generalized Garratt model to the present case.

(as in Stull (1988), for example). Eq. 2 is then approximated by[5]:

$$u\frac{\partial\theta}{\partial x} + w\frac{\partial\theta}{\partial z} = -\frac{\partial}{\partial z}\overline{w'\theta'} \tag{3}$$

under the assumptions that:

1. A steady state has been obtained so that the partial time derivative can be neglected;

2. Conditions are homogeneous in the y-direction, which is taken to be parallel to the coast;

3. Variations in the air density are negligible over the IBL;

4. Radiative effects within the IBL can be neglected; and,

5. Horizontal diffusion within the IBL can be neglected.

Assumption 3 is standard in mesoscale modelling, the small density variations being unlikely to be significant in this term relative to the uncertainties involved in determining $\overline{w'\theta'}$. Assumption 5 also appears to be a reasonable one. The assumptions that, in the IBL, variations of θ with fetch dominate over those in time and in y may not be valid under all mesoscale conditions. In the present case though, an inspection of potential–temperature contour plots argues that such an approximation should be a good one.

It is straightforward to test the validity of assumption 4 explicitly, since the low–level curvature of the potential–temperature profile provides an indication of the relative importance of turbulent and radiative cooling (André and Mahrt, 1981; Garratt, 1992). If turbulent cooling is dominant then near-surface air will be well mixed, leading to a positive curvature. By contrast, radiative cooling (which is often more important in a nocturnal boundary layer) gives rise to a negative curvature (André and Mahrt, 1981). An evolving boundary layer cannot be categorized quite so simply, but we can nevertheless test the curvature in the well-developed MIBL at large fetches. It is conveninent to work with a parameter introduced by André and Mahrt (1981),

$$\gamma = 1 - 2\frac{\theta(h/2) - \theta(0)}{\theta(h) - \theta(0)}, \tag{4}$$

where h is the stable boundary layer depth. This quantity has been observed to vary from -0.74 in a nocturnal boundary layer dominated by radiative cooling (André and Mahrt, 1981) up to 0.5 in the stable MBL discussed by Garratt and Ryan (1989). Results from the simulation are plotted in Fig. 4. They are clearly supportive of the assumption since $\gamma \to 0.67$ in the mature MBL.

[5]The vertical advection term is omitted by Garratt (1992) from the outset, by appeal to the assumption of Sec. 6.3.

On the subject of potential–temperature profiles within the MIBL, it seems appropriate at this stage to make a brief digression and consider the fits made by Mulhearn (1981) and by Garratt and Ryan (1989). The functional form

$$\frac{\theta - \theta(0)}{\theta(h) - \theta(0)} = (z/h)^n \tag{5}$$

was used, Garratt and Ryan (1989) obtaining $n = 2$ in contrast to Mulhearn's (1981) $n = 1/4$. The fact that Mulhearn's fit was made at smaller fetches led Garratt (1990) to speculate that the curvature (and hence n) might be changing rapidly at short fetches. We can rewrite Eq. 5 to define n as a function of position through

$$n = \frac{z}{\theta - \theta(0)} \frac{\partial \theta}{\partial z}. \tag{6}$$

A cross section of n values is shown in Fig. 5. A good fit would be indicated on such a plot by a region of slowly–varying n. While not being inconsistent with the values found previously (Garratt, 1987; Mulhearn, 1981), the results from this simulation do not lend themselves well to a fit of the form of Eq. 5. Using a fairly small n, a fit might be tenable in the lower part of the MIBL but is quite unrealistic in the upper part.

6.1 Validity of the $\partial\theta/\partial x$ Assumption

A key assumption in Garratt's model is that

$$\frac{\partial \theta}{\partial x} \approx -\frac{\partial \theta}{\partial z} \frac{dh}{dx}. \tag{7}$$

Garratt (1987) proposes an argument for the validity of this assumption at the height $z = h$. However, the same assumption is subsequently used (Garratt, 1987; Garratt and Ryan, 1989) without any justification in order to approximate $\partial\theta/\partial x$ for all heights up to and including h (this occurs when Eq. 7 is used in an integral from ground level up to height h). Consider the variation in potential temperature as one moves along a line $z(x)$, letting s denote the distance travelled along the line.

$$\frac{d\theta}{ds} = \frac{\partial \theta}{\partial x} \frac{dx}{ds} + \frac{\partial \theta}{\partial z} \frac{dz}{ds} \tag{8}$$

Now, if along the boundary layer top ($z = h(x)$) the potential temperature is a constant then one immediately obtains the assumed relation,

$$\frac{\partial \theta}{\partial x} = -\frac{\partial \theta}{\partial z} \frac{dh}{dx}. \tag{9}$$

Furthermore, the same relation can be seen to hold along any line which is parallel to the boundary layer top ($z(x) = h(x) - \text{constant}$) provided

that the potential temperature is constant along that line. In this way the relation can be extended over the full IBL. Thus, the assumption amounts to a claim about the contours of potential temperature within the IBL — they have been taken to be a series of parallel lines, the uppermost of which is the boundary layer height itself.

Potential temperature contours within the simulated IBL are shown in Fig. 6. Despite some convergence of the contours towards the coast[6], Eq. 7 is seen to provide a good approximation.

6.2 Turbulence Assumption

Garratt's model deals with properties of the IBL in terms of the following dimensionless functions:

$$\begin{aligned} f_1 &= u/U \\ f_2 &= \frac{\theta - \theta_{\rm surf}}{\Delta\theta} \\ f_3 &= w/w(h) \\ f_4 &= \frac{\overline{w'\theta'}}{(\overline{w'\theta'})_{\rm surf}} \\ f_5 &= \frac{u_\star^2}{(u_\star^2)_{\rm surf}} \\ f_6 &= v/V, \end{aligned} \tag{10}$$

with the normalizations being made through the parameters:

- U and V, the x and y components respectively of the ambient wind;
- $\Delta\theta$, the potential temperature difference between the overland mixed–layer air and the air at the sea surface; and,
- $\chi_{\rm surf}$, the variable χ evaluated at the sea surface.

The model (Garratt, 1987; Garratt and Ryan, 1989) assumes that these functions are self-preserving[7], depending only on $\lambda = z/h$. However, we are interested here in the possibility of allowing for variations with fetch. Integrating Eq. 3 between the ground and the boundary layer top, and

[6] The contour at the sea-surface temperature provides an approximation to the IBL top if this is defined through 'method 4' (see Sec. A.4). Method 4 cannot be used at small fetches, however, essentially because the air has not yet been able to cool sufficiently to reach that temperature at any height. Hence, Eq. 7 must break down at the smallest fetches.

[7] Unless the IBL height is a constant, independent of fetch, then the assumption of profile self-preservation is inconsistent with the assumption that lines of constant potential temperature are parallel. Use of both assumptions therefore requires an approximation within the terms of the model itself.

making use of Eq. 7, gives an ordinary differential equation for the IBL growth,

$$\frac{dh}{dx} = \frac{w(h)}{UB\Delta\theta} - A_0 \frac{(\overline{w'\theta'})_{\rm surf} - \overline{w'\theta'}(h)}{U\Delta\theta}, \tag{11}$$

where:

$$A_0^{-1} = \int_0^1 f_1 \frac{\partial f_2}{\partial \lambda} d\lambda \tag{12}$$

$$B = A_0 \int_0^1 f_3 \frac{\partial f_2}{\partial \lambda} d\lambda. \tag{13}$$

It is now assumed that turbulence at the IBL top is negligible compared to that at the surface, so that $\overline{w'\theta'}(h) \approx 0$. Alternatively, this may be expressed as $f_4(h) \approx 0$. In Garratt's simulations (1987), the assumption held "well away from the coast" (more than $\sim$ 50 km). Using the 1 1/2 order turbulence closure scheme of the Met. Office mesoscale model (Golding, 1986), the function f_4 can be evaluated as:

$$f_4 = \frac{K_h(\partial\theta/\partial z - \gamma_c)}{C_H v_1(\theta_1 - \theta_{\rm surf})}, \tag{14}$$

where the subscript 1 refers to the first model level and $\gamma_c = 3 \times 10^{-4}$ K/m is a slightly–stable lapse rate introduced as part of the model turbulence parameterization.

The function f_4 is plotted for various fetches in Fig. 7. There are some large variations at low altitudes[8] but at the IBL top (see Fig. 3) the assumption can be seen to be a good one so long as the fetch is not too small. Even for a fetch of $\sim$ 20 km, such an approximation may still be supportable, since $f_4 < 0.2$. Note that an increase in f_4 above the IBL at short fetches is attributable to residual convective turbulence.

6.3 Vertical Velocity

Another assumption of Garratt's model (Garratt, 1987; Garratt and Ryan, 1989) is that the vertical velocity at the IBL top is small. If $w(h) \ll U$ then the first term on the right–hand side of Eq. 11 (ie, the piece coming from the vertical advection term in Eq. 2) can be neglected. Vertical velocity profiles are plotted in Fig. 8. The strong offshore ambient wind pushes the sea-breeze circulation away from the coast and thus the profiles at shorter fetches ($x = -78$ and -39 km) exhibit uplift in front of the SBF. Profiles at larger fetches display subsidence throughout the IBL, the magnitude increasing

[8]Recalling that $f_4(0) = 1$ by definition, it is a little surprising to note that f_4 falls off sharply between the ground and the first w-grid level, before increasing towards a low level peak. This low–altitude decrease may be caused artificially by the model turbulence scheme, since a full turbulence calculation cannot be undertaken at the first level (Golding, 1986, Sec. 4.3).

with height. The magnitude of the vertical velocity is never larger than 0.5% of U throughout the IBL, which suggests that the assumption may indeed have some merit.

6.4 Heat Transfer Coefficient

The usual formulation of Garratt's model uses a critical layer flux Richardson number in obtaining an expression for $(\overline{w'\theta'})_{\rm surf}$. As pointed out by Garratt (1987) himself, however, an alternative formulation is simply to use the heat transfer coefficient C_H. Garratt (1987) defines a coefficient with reference to the geostrophic wind and the difference in potential temperature across the whole of the IBL, and with that definition the IBL growth is essentially controlled by C_H. It is more usual though to define C_H with respect to some fixed reference height. In the Met. Office mesoscale model, this is taken to be the first model level (Golding, 1986), so that:

$$(\overline{w'\theta'})_{\rm surf} = -C_H v_{H1}(\theta_1 - \theta_{\rm surf}), \tag{15}$$

v_H being the horizontal wind speed,$= \sqrt{u^2 + v^2}$. The MIBL growth equation then becomes:

$$\frac{dh}{dx} = A_0 C_H v_{H1} \frac{\theta_1 - \theta_{\rm surf}}{U\Delta\theta}. \tag{16}$$

A full calculation based on Eq. 16 will be considered later (Sec. 7.3). If we follow Garratt (1987) for a moment though, by assuming that A_0 is independent of fetch, the IBL growth will be governed by the surface heat flux. It is then encouraging to note that the qualitative behaviour of the heat flux accords with the expected IBL evolution. Fig. 9 suggests that the IBL will grow very rapidly over the first 50 km or so, after which the growth rate falls off significantly.

6.5 Critical Flux Richardson Number

A more common development of Eq. 11 uses the concept of a critical value of the layer flux Richardson number, $R_f = b/p$ where:

$$b \equiv \frac{-g}{\overline{\theta}} \int_0^h (\overline{w'\theta'}) dz \tag{17}$$

$$p \equiv \int_0^h \left(-\overline{u'w'}\frac{\partial u}{\partial z} - \overline{v'w'}\frac{\partial v}{\partial z} \right) dz. \tag{18}$$

In the expression for b, the potential temperature appearing outside the integrand should be interpreted as some average value, characteristic of conditions below h. An analogy between the stable MIBL and the nocturnal boundary layer (Garratt, 1987; Garratt, 1992) suggests a local scaling assumption whereby the IBL top can be associated with a critical value of

R_f (Nieuwstadt and Tennekes, 1981; Nieuwstadt, 1984). Denoting the ambient, geostrophic wind by G (with x and y-components U and V respectively) and substituting the dimensionless functions of Eq. 10 into the R_f definition, it is straightforward to derive Garratt and Ryan's (1989) equation for the surface heat flux[9]:

$$(\overline{w'\theta'})_{\rm surf} = -\frac{(u_\star^2)_{\rm surf} G R_f^{\rm crit}}{(g/\overline{\theta})hf}. \tag{19}$$

The factor f is calculable in principle, the following expression for the quantity having been presented by Garratt and Ryan (1989):

$$f({\rm Garratt\ and\ Ryan}) = h\int_0^1 f_4 d\lambda \left[\int_0^1 f_5 \frac{\partial f_1}{\partial \lambda} d\lambda\right]^{-1}. \tag{20}$$

If one is prepared to accept the assumptions that $\overline{w'\theta'}(h) \approx 0$ (Sec. 6.2), that $w(h) \approx 0$ (Sec. 6.3) and that profiles are self-preserving, then the final result of the Garratt model follows by substituting Eq. 19 into Eq. 11 and integrating over fetch. Doing so produces the well–known $h^2 \sim x$ equation (Eq. 1), with:

$$\alpha^2 = \frac{2A_0 G R_f^{\rm crit} (u_\star^2)_{\rm surf}}{U^3 f}. \tag{21}$$

As stated previously (see Sec. 5), in practice α has been regarded as a free parameter to be fit to the data. It has been suggested (Garratt, 1992) (and even more tentatively by Garratt (1990)) that differences between the values of α that are appropriate under different circumstances may be largely due to differences in the angle ϕ between the ambient wind and the coast. Since Eq. 21 can be recast (Garratt, 1987) as

$$\alpha^2 = \frac{2A_0 C_D^a R_f^{\rm crit}}{f\cos^3\phi}, \tag{22}$$

this suggestion implies that there is only modest variation in A_0, f and C_D^a, a drag coefficient which is set by reference to the ambient wind speed.

In fact, there are some additional assumptions implicit in the formula (Eq. 20) for f given by Garratt and Ryan (1989). A somewhat more general formula is as follows:

$$f = h\int_0^1 f_4 d\lambda \left[\int_0^1 f_5 \left(\cos^2\phi \frac{\partial f_1}{\partial \lambda} + \sin^2\phi \frac{\partial f_6}{\partial \lambda}\right) d\lambda\right]^{-1}, \tag{23}$$

where the angle ϕ is allowed to vary with height, such that

$$\tan\phi = v/u. \tag{24}$$

[9]Eq. 19 is given by Garratt and Ryan (1989) without the minus sign, clearly an error since $\overline{w'\theta'}$ must be negative in turbulent cooling. The sign has been subsequently corrected (Garratt, 1992).

The calculation of Eq. 23 has assumed that turbulence within the IBL is locally isotropic,

$$\frac{v'_H}{v_H} \approx \frac{u'}{u} \approx \frac{v'}{v}. \tag{25}$$

Our generalized result for f can be brought into agreement with Garratt and Ryan's expression if either of the following assumptions is made (neither of which is stated by Garratt and Ryan (1989)).

I. Velocity profiles within the IBL (when normalized by the corresponding ambient wind component) develop in the same way parallel and perpendicular to the coast, so that $\partial f_6/\partial z \approx \partial f_1/\partial z$.

II. Within the IBL, velocities parallel to the coast are always small, so that $\phi \approx 0$.

Neither of these assumptions are convincing as general statements, and are clearly not true in the numerical simulations (see Fig. 10). Of course, the factor f is not calculated in practice but is simply absorbed into the fit coefficient α. Thus, our arguments do not bring into question the use made of Eq. 1 in the literature, but we have nevertheless discussed the matter because it is important to be explicit about the assumptions upon which a model is based.

7 Analysis Using Garratt's Model

Insights into the evolution of the simulated MIBL are revealed by applying a generalization of Garratt's model. Quantities in the model that are swept up into the fit coefficient can in fact be calculated explicitly at each grid point. A numerical integration of Eq. 11 is performed, allowing the model parameters to vary with fetch. This enables the model to capture more detailed information about the MIBL growth.

7.1 The Dimensionless Functions

The dimensionless function f_4 has already been described in Sec. 6.2 and an un-normalized form of f_3 was discussed in Sec. 6.3. Here, we describe results for f_1, f_2, f_5 and f_6.

In the formalism of Garratt's model, the x axis is taken to be perpendicular to the coast. This means that along the simulation grid line $y = -54$ km, where our attention is focused, the horizontal axes defined by the Garratt model are coincident with the axes chosen for the numerical simulation (see Fig. 2). The required u and v wind components are therefore as specified by the numerical model, and so the functions f_1 and f_6 can immediately be evaluated. They have been plotted in Fig. 10. The negative values of f_1 seen at low altitudes are indicative of a sea breeze. However, since the

strong off-shore wind pushes the sea-breeze circulation away from the coast, there is no indication of a sea breeze in the plot at ~ 20 km fetch.

Function f_2 is the scaled θ profile, the curvature of which was discussed in Sec. 6. The scaled profile is plotted in Fig. 11, the parameter $\Delta\theta$ of Eq. 10 having been set to 9 K. In the mature MIBL, one can classify four regions of potential temperature behaviour:

1. A region starting at the surface where the potential temperature is almost constant, increasing only slowly with height.

2. An inversion.

3. A region extending up to ~ 1500 m in which the potential temperature increases with height but more slowly than in region 4. This transitional region is presumably what remains of the decaying overland convective boundary layer.

4. A region at high altitudes, above the planetary boundary layer, in which potential temperature increases with height.

As the MIBL becomes better established with increasing fetch, a surface–based inversion is developed first (see the profile at $x = -78$ km) and is then elevated as region 1 is developed.

Finally, in Fig. 12, we show the turbulent velocity function f_5. It is calculated in terms of model variables from:

$$f_5 = \frac{K_m \partial v_H / \partial z}{C_D v_{H1}^2}. \tag{26}$$

Similar comments apply here as for the buoyancy function f_4 (see Sec. 6.2). There are large variations at low altitudes but in general $f_5 \to 0$ towards the top of the IBL. An exception occurs above the IBL at short fetches and is due to residual overland turbulence.

7.2 Model Integrals

The Garratt model contains various parameters which are calculated from integrals over the depth of the IBL. Such integrals will obviously depend on the definition of the IBL top, the self-consistent value to use being that determined from the integration of Eq. 11. It is sufficient for the present though to use MIBL heights deduced from the simulation results. This should reveal whether or not the generalized form of the Garratt model is capable of reproducing any of the variation in growth rates evident from the simulation.

The integrals have been evaluated by first constructing a fit for each function f_i as described in Appendix A. The derivatives of f_i and all of the necessary integrals could then be calculated analytically.

We begin with the factor A_0, defined by Eq. 12. First, let us note that the combination $A_0 f^{-1}$ takes the place of a parameter A in the original model formulation of Garratt (1987). In that simpler approach, A is defined by taking $f = 1$ and by setting $f_1 = 1$ in Eq. 12 (ie, assuming $u \approx U$). For the situation modelled by Garratt (1987), A was found to be a constant ≈ 1.8. Fig. 13 shows that in our case A increases with fetch, tending towards Garratt's value. Since dh/dx is proportional to A in this version of the model (Garratt, 1987), it is clear that variations with fetch are potentially important in understanding the MIBL growth mechanism. (In fact, variations in A are related to deviations from the model assumption (Sec. 6.1) that the potential temperature is a constant along the boundary layer top. By definition,

$$A = \frac{1}{f_2(h)} = \frac{\Delta\theta}{\theta(h) - \theta_{\mathrm{surf}}}. \tag{27}$$

Thus, A will change if $\theta(h)$ does. Values for the potential temperature difference between the surface and the IBL top can be seen in Fig. 13.)

The parameter A_0 (Eq. 12) from the full version of Garratt's model (Garratt and Ryan, 1989; Garratt, 1992) is shown in the upper plot of Fig. 14. In a typical MIBL one expects to find off-shore velocities throughout and hence (since f_2 is monotonic) a positive value for A_0. However, on-shore velocities may be encountered in the presence of a sea breeze. Such on-shore flow will occur at low altitudes, the prevailing off-shore flow being re-established within the return current of the sea-breeze circulation. In order for A_0 to remain positive in that case, the IBL height appearing in the integral must somewhat exceed the height at which the wind becomes off-shore. (Note that the difference between the heights need not be large since the A_0 integral is dominated by the inversion region around the IBL top where $\partial f_2/\partial z$ is strong.) Should the value of h not be large enough then a transition from a negative to a positive integral will occur at a fetch within the sea-breeze circulation. This leads to an unphysical singularity in A_0, and hence also in dh/dx. Using IBL heights derived from the simulation, such a transition does not occur and so A_0 remains well behaved. However, if one were to take heights from, say, the middle rather than the top of the inversion ('method 2' of Appendix A) then a singularity would indeed occur, as shown by the lower plot of Fig. 14.

In a case where A_0 has a singularity then the Garratt model can only be applied beyond the singular point, at fetches sufficiently large to be outside the range of the sea-breeze circulation. The alternative, where A_0 remains positive, requires that for all fetches there exists an offshore wind within the designated IBL. In this case, the effect of the sea breeze is to increase A_0, as seen in Fig. 14. This implies more rapid MIBL growth, particularly in the region around the sea-breeze front. The sea breeze slows down some of the flow in the MIBL and thus allows the air extra time (for a fixed distance

travelled) in which to become adjusted to the change in surface conditions. If retarded air exists close to the top of the MIBL, where the growth mechanism operates most strongly[10], then the growth rate could be unusually high. Such an explanation for the MIBL perturbation is clearly attractive at a qualitative level, but it remains to be seen whether the variations found in A_0 are able to provide a reasonable quantitative description via Eq. 11. Indeed, the integration of Eq. 11 through the sea-breeze circulation may not be valid at all, since it could quite conceivably generate a singularity.

We next consider the parameter B from Eq. 11. In the upper plot of Fig. 15, results are shown for the integral in Eq. 13, with f_3 being unnormalized. The integral is positive at short fetches, since uplift occurs, but becomes negative further out to sea due to subsidence within the sea-breeze circulation. With f_3 normalized, the results for B itself (the lower plot of Fig. 15) are complicated by the presence of a singularity where $w(h) \to 0$. Since B occurs in Eq. 11 only in the combination $w(h)/B$ such a singularity represents a vanishing contribution to the model growth rate and is perfectly acceptable. B/A_0 is positive in general, a property which must hold if the vertical velocity has the same sign throughout the IBL. Negative values can be found, however, near to the $w(h) \to 0$ singularity position, if the change from uplift to subsidence within the IBL occurs at different fetches for different heights. In these circumstances, a problem arises in Eq. 11 since there will exist at a point where $B = 0$ but $w(h) \neq 0$ and the first term is singular. Thus, the contribution to MIBL growth from the vertical advection term of the potential–temperature equation is dangerous *in the form in which this contribution has been derived.* In practice, the vertical advection term does not contribute significantly to the understanding of MIBL growth provided by the framework of Garratt's model. Hence, the appropriate course is to follow Garratt (1992) and drop this term from the model altogether.

Finally we consider the parameter f, which appears in the R_f formulation of the model. Unfortunately, it has not been possible to obtain sensible results when attempting to evaluate Eq. 23 (in particular, there are large fluctuations in the results for neighbouring grid points). This has certainly not been helped by numerical difficulties associated with the very rapid variations in f_4 and f_5 between vertical grid points. The main problem though is the need to approximate the behaviour of functions between the ground and the lowest model level. Altitudes below 10 m are very important in the calculation of f since the vertical derivative of the wind speed is very strong there. A realistic explicit calculation of f would therefore require detailed knowledge about changes in wind speed very close to the ground, beyond that provided by a mesoscale numerical model. Even if tackled through theory, the issue would be significantly complicated by the presence of the sea

[10]Recall that Eq. 12 is dominated by the contribution from the inversion.

breeze.

7.3 Modelling the Observed Growth

The integration of Eq. 11 requires the specification of an initial condition, $h_0(x_0)$. From the discussion of the previous section, it is known that the IBL height when the sea-breeze system is encountered will be extremely important — if the height is not large enough, then A_0 will be singular and the model will break down. Thus, there may be a sensitivity to the initial condition chosen, a point which is considered in Appendix B. It is sufficient here though to note that there exist reasonable choices of the initial condition such that A_0 is always positive and the model remains valid. Moreover, the results vary remarkably little whenever a choice is made that leads to a valid model.

In Fig. 16, the IBL height calculated from the integration of Eq. 11 is presented. The results are in good agreement with the profile deduced from the mesoscale model simulation. On either side of a short region where there is rapid growth, the growth rates predicted by the generalized Garratt model are quite small. This makes the period of rapid growth a very distinctive feature. In producing the results of Fig. 16, we have taken on board the assumptions of Secs. 6.2 and 6.3, including only the second term in Eq. 11. The inclusion of the other terms has been explicitly tested and was found to have little effect[11].

8 Effects of the Sea Breeze Circulation on the MIBL

The picture emerging from our generalization of Garratt's model is that the unusual pattern of simulated MIBL evolution can be explained through an interaction of the sea-breeze circulation with the normal mechanism of IBL development. Most notably, retardation of the offshore wind by the sea breeze can produce air over the sea which is almost static. Such air has plenty of opportunity to become adjusted to the change in surface conditions. This enables a well-developed marine boundary layer to be established within a very short distance. Our analysis so far has concentrated on the MIBL evolution along one particular line at one particular time. In this section, we attempt to promote this picture to a more general status, by discussing the behaviour at other times and places.

It is interesting to consider the MIBL evolution between the coast and the SBF. In Fig. 17, the wind induced by the sea-breeze circulation along $y = -54$ km at 1500 hr is plotted, an 'induced wind' having been calculated

[11] Although B changes sign, and the first term in principle contains a singularity, when the term was evaluated at the grid points, B was always sufficiently large for the first term to be small. Our evaluations of the first term support the contention of Sec. 6.3 that non-turbulent vertical advection is not important in establishing the MIBL.

from the difference between the simulated wind and the input ambient wind profile (Plant and Atkinson, 1999). Also shown on the figure is the MIBL height. At short fetches, up to $x \sim -70$ km, the ambient wind is very little altered by the sea-breeze circulation. Significantly, the MIBL evolution at such fetches is well represented by an equation of the standard $h \sim \sqrt{x}$ form (see Fig. 18). The MIBL at 1300 hr and 1400 hr can also be seen to agree with the same $h \sim \sqrt{x}$ equation, up to the fetch where the sea breeze is encountered. This fetch decreases over time since the SBF is moving inland. It appears that the MIBL develops according to the standard mechanism between the coast and the SBF, but then grows very rapidly within the sea-breeze circulation itself.

The coefficient of the $\sqrt{x}$ curve in Fig. 18 implies that $\alpha = 0.0215$ using Garratt's growth equation[12]. This may be compared with the value $\alpha = 0.024$ found in the aircraft observations presented by Garratt and Ryan (1989). Alternatively, if one corrects for the wind angle[13] to obtain an equivalent value for flow perpendicular to the coast, then $\alpha_\perp = 0.0110$ here, almost identical to Garratt's (1987) $\alpha_\perp = 0.0113$ proposed from a numerical simulation. Although the sea-breeze circulation may influence the pattern of MIBL development, one would not expect it to affect the equilibrium MBL height. Thus, it is important for the validity of our interpretation that an extrapolation of the short–fetch $\sqrt{x}$ behaviour should approach the equilibrium height within a fetch of few hundred kilometres or so. For fetches of ~ 300 to 400 km, the extrapolation yields h in the range 260 to 300 m, which is smaller than the simulated equilibrium height, but certainly not implausible.

Comparing Figs. 17 and 19, it is clear that the sea breeze becomes stronger between 1400 hr and 1500 hr. This can be linked to the change in the MIBL profile, in which a diffuse rapid–rise region in the vicinity of the sea breeze at 1400 hr is tightened up into the familiar step–like feature at 1500 hr. At 1400 hr the presence of retarded air within the sea-breeze circulation enables the MIBL to deepen more rapidly than would otherwise be the case. However, at this time there is no need for the sort of extreme growth rate which is required at 1500 hr in order to ensure that offshore velocities occur below the IBL top.

Later in the day, a situation can arise where the SBF is very close to the coast. It is then possible to develop a mature MBL almost immediately, a region of extreme growth occurring within a very short fetch. A good example of this phenomenon is shown in Fig. 20 along the line $y = -69$ km at 1600 hr. The position of the coast for this line is at $x = -99$ km.

Later still the SBF crosses over the coast and acts to move marine air over

[12]This value is obtained by substituting $U = 12\text{ms}^{-1}$, $\Delta\theta = 9$ K, $\overline{\theta} = 297$ K and $g = 9.8$ ms^{-2} into Eq. 1.

[13]ie, taking account of the $\sec^3 \phi$ factor in Eq. 22.

the land. By this time, a mature MBL exists at all positions over the sea, as can be seen in Fig. 21, which shows a cross-section of potential temperature along the line $y = -39$ km at 1800 hr. The coast is at $x = -75$ km along this line.

The changes in potential–temperature profiles with time are shown in Figs. 22 and 23 at a point out to sea and at a point just inland respectively. At the point ≈ 20 km out to sea, during the afternoon an MIBL is in an intermediate stage of development. It becomes slightly thicker over time as a sea-breeze circulation becomes established and starts to move towards the coast. Air above the point is slowed down a little as the afternoon progresses, allowing a little more time for it to react to the change in surface conditions. The SBF passes the point at about 1600 hr. By 1700 hr the point is contained with the heavily–retarded, almost stationary region of air just behind the front. An MIBL can grow extremely rapidly under such circumstances, leading to profiles at 1700 hr and 1800 hr that are typical of a mature MBL with depths of ~ 350 to 400 m. For the point which is just inland (Fig. 23), the potential–temperature profiles are characteristic of a deep, convective boundary layer which becomes gradually warmer during the day. Between about 1700 hr and 1800 hr, however, the SBF passes the point, bringing in marine air and so producing a profile at 1800 hr that is more typical of an MBL. If there continues to be a significant onshore flow, such a profile will become modified by the high overland temperature and a convective IBL will develop.

The changes in boundary layer structure seen in Figs. 22 and 23 can thus be interpreted straightforwardly, using the idea that MIBL growth can be enhanced in the vicinity of a sea breeze. The idea provides a smooth description for the behaviour observed when flow changes from off to onshore. Indeed, the need for a coherent description of this transition implies that there *must* exist some interaction between the sea-breeze circulation and MIBL development. In particular, the interaction enables one to explain the presence of a well-developed MBL immediately offshore of the coast at the time just before the flow at the coast reverses direction. The air advected over land by the sea breeze at a height of a few hundred metres or so is clearly seen to be typical of marine conditions and is able to generate an IBL over land. The standard picture of an MIBL is inappropriate under these circumstances since a $h \sim \sqrt{x}$ MIBL cannot suddenly turn into the source for such an onshore flow.

9 The Low Wind Case

It might be expected that the interaction between the sea-breeze circulation and the normal mechanism of MIBL development would also be important in the low wind case. Although hints of an interaction can be found, as

pointed out by Plant and Atkinson (1999), it has proved difficult to identify unambiguous phases of rapid growth. In the low wind case the SBF is found very close to the coast or else over land. For example, Li and Atkinson (1998b) report that the SBF has just crossed the coast by 1400 hr along $y = -54$ km. By contrast, the dramatic demonstrations of the interaction in the high wind case occurred where the SBF was a significant distance offshore so that there was a definite region of 'normal' IBL growth between the coast and SBF.

Another issue is the vertical resolution, since the fully–developed MBL in the low wind case has a depth of ~ 100 m, which translates into just 10 vertical grid points[14]. This makes it difficult to obtain detailed information on the variations within the growing IBL. Indeed, a full analysis of the low wind IBL growth would probably require further improvements to the vertical resolution.

Nonetheless, the unusual pattern of evolution of contours of water vapour and refractivity identified by Plant and Atkinson (1999) can be explained as a consequence of the sea breeze. In Fig. 24, the $q = 12$ mb contour along $y = -54$ km at 1500 hr is shown, superimposed over a plot of the wind. The behaviour of the contour beyond $x \sim -50$ km is much as might be expected, the MIBL moistening gradually as the fetch increases. Between this point and the coast, there is a strong sea breeze which moistens the near–surface air by bringing in moist marine air from further out to sea. A slight dip in the water vapour contours just after the coast may be due to some subsidence after the SBF.

10 Conclusions

Phase 1 of this project (Li and Atkinson, 1998b; Atkinson and Li, 1999) was successful in simulating many features of the propagation environment, in agreement with aircraft observations (Brooks *et al.*, 1997; Brooks *et al.*, 1999). An MIBL, of realistic depth, resulted from the flow of hot, dry air from Saudi Arabia over the Persian Gulf. The simulations also generated a sea-breeze circulation. Although this was located outside the observation region, its existence is supported by general arguments (Atkinson and Li, 1999), including many observations that have been made under similar conditions (Atkinson, 1981). However, the simulations run for phase 1 were not able to detect any of the short–scale (10 to 20 km) horizontal variations in the mature MBL that were found in the aircraft observations.

The phase 1 simulations used 33 vertical levels and a horizontal grid length of 6 km. In the present report, the numerical resolution has been

[14]There were only 6 vertical grid points in the first 100 m of runs performed previously (Li and Atkinson, 1998b; Atkinson and Li, 1999; Plant and Atkinson, 1999), which used 33 levels in total.

enhanced in an attempt to capture short–scale variations. Taking 41 vertical levels and a 1 km horizontal grid length, there was no evidence for such variations in the mature marine boundary layer (MBL). The observed short–scale variations can therefore not be explained with the mesoscale model as it stands.

The enhanced resolution has revealed some unusual perturbations in the developing MIBL, which have a significant effect on the refractivity environment within $\sim$ 100 km of the coast. We believe that the perturbations are genuine and observable phenomena, which have a simple physical interpretation. They are caused by the presence of the strong sea-breeze circulation, which modifies the MIBL growth mechanism. In the low wind case, the MIBL just out to sea is very moist, due to the on-shore flow of the sea breeze which transports marine air towards the coast. In the high wind case, there is little onshore flow, but the sea-breeze circulation strongly retards the prevailing offshore wind. For a fixed distance travelled the retarded air has additional time in which to respond to the change in surface conditions. This can lead to an extremely rapid deepening of the MIBL. Our interpretations are based on qualitative arguments, a detailed analysis of the simulation results and a generalization of an established MIBL analytic model.

Appendices

A Definition of the IBL Height

As noted in the main text, the height of a stable IBL can reasonably be defined in various ways. In this Appendix, we consider the application of some of the methods commonly found in the literature to the results from our numerical simulations. The usual reason for adopting a particular definition is simply that of convenience, subject only to the conditions that a consistent method should be used and that it should produce a credible height.

For each of the methods to be described, either of two approaches may be followed. In the first approach, only the raw data values at the grid points are used. In the second approach, a numerical fit to is made to the grid point values. If f is some property specified at the grid points, then $f(z)$ is represented by:

$$f(z) \approx \sum_{i=0}^{n} c_i T_i \left(\frac{2z - z_{\min} - z_{\max}}{z_{\max} - z_{\min}} \right), \quad z_{\min} < z < z_{\max}, \tag{28}$$

where T_i is a Chebyshev polynomial of the first kind. This is a standard numerical technique, and a NAG routine is available for determining the coefficients $\{c_i\}$, by making a least–squares fit to the grid values in the fit range. The fit range has been taken to be the first 30 model levels[15] and n has been set to 15. Having made such a fit, vertical derivatives and integrals of the fit functions (and the products of such functions) can then be calculated analytically. For example,

$$\frac{\partial f}{\partial z} \approx \sum_{i=0}^{n} c_i \frac{d}{dz} T_i \left(\frac{2z - z_{\min} - z_{\max}}{z_{\max} - z_{\min}} \right) = \sum_{i=0}^{n-1} d_i T_i \left(\frac{2z - z_{\min} - z_{\max}}{z_{\max} - z_{\min}} \right), \tag{29}$$

where each d_i is a known function of $\{c_i\}$. In practice, the first approach has been used essentially as a check on the application of the second. Increments in z made while searching for an IBL height are such that there are ten equally–spaced heights considered between each pair of grid levels.

Unless otherwise stated, the accompanying figures show the results obtained by applying the various methods along the line $y = -54$ km at 1500 hr in the high wind case. Data from a run with a 3 km grid length were used. A summary of the results is provided by Fig. 25, in which results from some of the grid points have been omitted from the curves. This is because some of the methods tested were found to produce unacceptable heights at some fetches.

[15] Either the p grid or the w grid may be used, as is appropriate for the property in question.

A.1 Method 1

In this method we look for a critical value of $\partial\theta/\partial z$, from the lowest model level upwards. The same basic approach has been used by Physick *et al.* (1989) and by Anthes (1978), taking a critical value of 1 K/km. This was satisfactory for well–mixed IBLs formed when sea air is advected overland, but the vertical gradients found in the MIBL are much stronger and a critical value of 15 K/km has been used here.

The results are shown in Fig. 26. Method 1 is unable to detect the existence of a boundary layer for fetches $\lesssim$ 65 km. This can be explained from the potential–temperature profiles at various x values, which are also shown in Fig. 26. The overland profile at $x = -153$ km seems reasonable. A little way after the coast, at $x = -78$ km, turbulent cooling has removed the overland surface layer but there has only been a partial adjustment to sea-surface conditions and so the well-developed MIBL profile seen at $x = 57$ km is not yet fully in evidence. At short fetches the potential temperature gradient exceeds the critical value from the very first model level. Fig. 26 also illustrates the fact that in a mature MIBL, method 1 determines the IBL height from the base of the inversion.

A.2 Method 2

Method 2 identifies the IBL height with the maximum value of $\partial\theta/\partial z$. In the mature IBL, this corresponds to the middle part of the inversion, as illustrated in Fig. 26. Results obtained using method 2 are shown in Fig. 27. It is marginally more successful than method 1 in determining a suitable IBL height at small fetches. Using method 1, there was no boundary layer detected at all until $x = -33$ km. Although method 2 will always produce a height, there is an artificial jump in value (from $\sim$ 45 to $\sim$ 195 m) at $x \sim -50$ km. Since the heights after the jump are apparently sensible, method 2 does at least manage to extend the range in which an appropriate IBL height can be detected. In order to ascertain the reason for this jump, potential temperature profiles are shown in Fig. 27 for the grid points just before ($x = -51$ km) and just after ($x = -48$ km) the jump.

Recalling the interpretation of Sec. 7.1, the jump in the IBL height calculated by method 2 can be seen to occur at the fetch where distinct regions 1 and 2 can first be distinguished. Just after the jump, both regions can be seen and method 2 yields the height near the middle of the inversion region. Just before the jump one can see a hint of a structure which will become the divide between regions 1 and 2. The strongest potential–temperature gradient occurs around this dividing height.

A.3 Method 3

This method is very similar to that of method 1. However, the search for a critical potential–temperature gradient is here made from the top down rather than the bottom up. As is illustrated in Fig. 26, method 3 determines the IBL height as being at the top of the inversion. The critical value for $\partial\theta/\partial z$ is set at 15 K/km, just as for method 1. Good results for all fetches are obtained using this method (Fig. 3), which has been adopted for the main body of the report.

In Sec. 7.1 the potential–temperature profiles were divided into four distinct regions. Some evidence supporting that classification is provided by Fig. 28, which shows the differences in IBL heights calculated by methods 1, 2 and 3. Provided that the fetch is large enough for the each of the determinations to be meaningful, the total inversion depth (represented by the difference $h_3 - h_1$ between the heights calculated by methods 3 and 1) remains almost constant with fetch and the IBL grows by means of elevating the inversion structure. The strongest gradients are found near the middle of the inversion structure (the method 2 height, $h_2 \approx (h_1 + h_3)/2$), although there is a tendency for the gradient maximum to fall gradually towards the base of the inversion.

A.4 Method 4

This method follows the approach of the Met. Office mesoscale code in determining a boundary layer depth for use in initialising the turbulent kinetic energy (TKE) (Golding, 1986). A reference line with gradient 0.3 K/km is drawn through the surface–level value of θ and the boundary layer top defined where this line first crosses the actual $\theta(z)$ profile. As can be seen in Fig. 29, the method has problems at small fetches. The reason for this can be illustrated using two potential–temperature profiles from the low wind case (the lower plot of Fig. 29). It is immediately apparent that the gradient of the reference line is very shallow, and that it would make little difference if the method were to simply identify the IBL height with the first height above ground at which the surface temperature is attained. At small fetches (for instance at $x = -78$ km in the figure), adjustment to the sea-surface temperature is incomplete and this temperature is only attained at sea level itself. The method is unable to deduce an IBL height under such circumstances.

A.5 Method 5

It is clear from the lower plot of Fig. 29 that it is not possible to draw a suitable reference line through the surface temperature which can be used to determine an IBL height at both short and long fetches. For example,

a reference line has been tried which is drawn through the potential temperatures at the surface and at the model top. The results obtained are not reproduced here, being qualitatively similar to those of method 4 (the IBL height is a little larger and reliable results can be found at marginally smaller fetches).

The philosophy behind method 5 is similar to that of method 4 in that the intersection point is again found of the potential–temperature profile with a specified reference line. The aim of method 5, however, is to investigate whether or not one can construct a suitable reference line solely from the conditions at high altitudes. The potential temperatures and gradients at the highest altitudes in the model remain almost unaltered from the specification in the initial conditions (Plant and Atkinson, 1999). A reference line is therefore drawn with the appropriate gradient through the potential temperature at the model top.

Results produced by method 5 can be seen in Fig. 30. Although some of the results at the smaller fetches do not seem untenable, the calculated IBL heights at larger fetches are obviously too high. Unrealistically large values occur when the reference line misses the inversion structure entirely, as illustrated in the lower plot of Fig. 30. In such a situation the reference line may be close to and almost parallel with the model profile above the inversion, giving rise to significant errors in ascertaining the precise position of intersection. This would explain the artificial jumps and fluctuations seen in Fig. 30.

A.6 Method 6

An alternative means of defining an IBL height that has been used in the literature is based on the vertical profile of TKE (Stunder and SethuRaman, 1985; Arritt, 1987; Garratt, 1990). This reaches a local minimum at the IBL top.

Example TKE profiles are shown in Fig. 31. In the well-developed IBL at $x = 57$ km, the TKE increases close to the ground, leading to a low–level maximum which decays towards the IBL top. Thus, the IBL height can be defined to be the altitude where the TKE is reduced to a small value (less than 1×10^{-4} m^{2}s^{-2}). At shorter fetches, however, the strong overland turbulence still persists, giving significant turbulence above the IBL. The criterion of method 6 is not appropriate for these fetches, and, as shown in Fig. 31, is unable to produce a realistic IBL height[16]. Faced with the short–fetch TKE profiles, it would be more appropriate to define an IBL through the local minimum in TKE. However, such a scheme could only be applied at the short fetches since the minimum disappears as the fetch increases. A combination of the two definitions is also unacceptable, since it generates

[16]The criterion is not met within the lowest 30 model levels, which causes the algorithm to return an IBL height of zero.

an artificial dip in the IBL height where the switch between methods has to be made.

B Initial Conditions in the Growth Equation

As noted in Sec. 7.3, integration of Eq. 11 may be sensitive to the initial condition chosen. In this Appendix we investigate that point by considering possible initial conditions for integration along the line $y = -54$ km at 1500 hr in the high wind case.

As discussed in Sec. 7.2, the generalized Garratt model will break down unless the quantity A_0 remains positive. If the model does remain valid, then it is expected that A_0 will become large around the position of the SBF. Because of the form of A_0 (see Eq. 12), a small error in the value of h at a grid point where A_0 becomes large could generate a significant error in the calculated A_0, and hence in the value of h predicted at the next grid point. Thus, the implementation of the model may fail for purely practical reasons. This could occur if an update to the MIBL height had been an significant overestimate, since there is no capacity in the model for a subsequent reduction of h. By contrast, a limited degree of numerical undershooting in the strong–growth region may not be so serious a problem. At the fetches where the MIBL grows quickly, an underestimate of h at one grid point will tend to produce an overestimate of A_0 (and hence of the growth rate) at the next. However, if an undershooting error is large enough then A_0 at the following grid point may be evaluated as negative, in which case the model implementation will be subject to an artificial break down.

Results obtained for the mature MBL height under different initial conditions are plotted in Fig. 32. Initial heights were varied from 1.0 m up to 200 m in 0.2 m intervals, while initial x positions ranged from the first grid point after the coast ($x = -96$ km) up to $x = -60$ km. The model always broke down if subsequent grid points were used. For most of the initial conditions tried, integration was invalid. However, there are three regions of Fig. 32 where Eq. 11 could be integrated over all fetches:

1. A band extending from $(x_0, h_0) \sim (-95, 50)$ to $\sim (-60, 90)$.
2. A band extending from $(x_0, h_0) \sim (-95, 140)$ to $\sim (-60, 180)$.
3. A triangular region in the top left–hand corner of the figure.

Within each of these regions, a mature MBL height was evaluated that changed remarkably little as the initial conditions varied. This can be seen from Fig. 33, which gives a scatter plot of the mature MBL heights. For the great majority of initial conditions where integration was valid, the mature MBL height was calculated to be in the range 362 to 362.5 m. There were no results below 362 m, which confirms that the calculations could cope with

some numerical undershooting. However, overshooting caused difficulties on the boundaries of the valid regions. This explains why the regions are marked by "fuzzy" edges in Fig. 32.

The banded structure can be explained using Fig. 34, which shows the full MIBL evolution using several initial conditions. For conditions below region 1, the MIBL height is not large enough for A_0 to remain positive once the sea breeze is encountered. Such initial conditions are therefore physically unacceptable, as discussed in Sec. 7.2. Within the valid regions, there are obvious differences in the MIBL evolution before the point of rapid growth, but excellent agreement from then on. Between regions 1 and 2 (and again between regions 2 and 3) the model appears to break down through undershooting at the first grid point where rapid growth is expected. The calculated growth rate at this grid point is found to be too low for a valid determination of A_0 at the following grid point.

Thus, the bands in Fig. 32 are a numerical artefact. If the right–hand side of Eq. 11 could be evaluated at any x position (rather than just at the grid points) and with complete accuracy (ie, without recourse to any of the interpolation in the vertical that is necessary in order to calculate model quantities from vertical integrals) then the generalized Garratt model would be found to be valid over a single, large region in (x_0, h_0) space.

References

André, J. C. and Mahrt, L. 1981. The Nocturnal Surface Inversion and Influence of Clear–Air Radiative Cooling. *J. Atmos. Sci.*, **39**, 864–878.

Anthes, R. A. 1978. The Height of the Planetary Boundary Layer and the Production of Circulation in a Sea Breeze Model. *J. Atmos. Sci.*, **35**, 1231–1239.

Arritt, R. W. 1987. The Effect of Water Surface Temperature on Lake Breezes and Thermal Internal Boundary Layers. *Bound. Lay. Meteorol.*, **40**, 101–125.

Atkinson, B. W. 1981. *Mesoscale Atmospheric Circulations.* Academic Press, London. 495pp.

Atkinson, B. W. and Li, J.-G. 1999. *Numerical Modelling of the Propagation Environment in the Atmospheric Boundary Layer over the Persian Gulf.* submitted to J. Appl. Meteorol.

Ballard, S. P. and Golding, B. W. 1991. *Short Range Forecasting Research, Mesoscale Documentation Paper No. 4 — Basic Model Formulation.* Tech. Rept. Met. Office. documenation paper version 1.5.1, 44pp.

Brooks, I. M., Rogers, D. P. and Goroch, A. K. 1997. *SHAREM-115 Observations: Atmospheric Environmental Data Collected by the UK Meteorological Research Flight C-130 Hercules Aircraft.* unpublished report available from ftp://megan.ucsd.edu/pub/sharem, 53pp.

Brooks, I. M., Goroch, A. K. and Rogers, D. P. 1999. Observations of Strong Surface Radar Ducts over the Persian Gulf. *J. Appl. Meterol.*, **38**, 1293–1310.

Garratt, J. R. 1987. The Stably Stratified Internal Boundary Layer for Steady and Diurnally Varying Offshore Flow. *Bound. Lay. Meteorol.*, **38**, 369–394.

Garratt, J. R. 1990. The Internal Boundary Layer — A Review. *Bound. Lay. Meteorol.*, **50**, 171–203.

Garratt, J. R. 1992. *The Atmospheric Boundary Layer.* Cambridge University Press. 316pp.

Garratt, J. R. and Ryan, B. F. 1989. The Structure of the Stably Stratified Internal Boundary Layer in Offshore Flow over the Sea. *Bound. Lay. Meteorol.*, **47**, 17–40.

Golding, B. W. 1986. *Short Range Forecasting Research, Mesoscale Documentation Paper No. 9 — Turbulent Diffusion.* Tech. Rept. Met. Office. 62pp.

Hsu, S. A. 1983. On the Growth of a Thermally Modified Boundary Layer by Advection of Warm Air over a Cooler Sea. *J. Geophys. Res.*, **88**(C1), 771–774.

Hsu, S. A. 1989. A Verification of an Analytical Formula for Estimating the Height of the Stable Internal Boundary Layer. *Bound. Lay. Meteorol.*, **48**, 197–201.

Li, J.-G. and Atkinson, B. W. 1997a. *Numerical Modelling of the Propagation Environment in the Atmospheric Boundary Layer Over Coastal Areas: Literature Review and Mesoscale Model.* Tech. Rept. 1. MoD Agreement NNR/2042/1. 36pp.

Li, J.-G. and Atkinson, B. W. 1997b. *Numerical Modelling of the Propagation Environment in the Atmospheric Boundary Layer Over Coastal Areas: Model Sensitivity Study.* Tech. Rept. 2. MoD Agreement NNR/2042/1. 69pp.

Li, J.-G. and Atkinson, B. W. 1998a. *Numerical Modelling of the Propagation Environment in the Atmospheric Boundary Layer Over Coastal Areas: Idealised Case Study.* Tech. Rept. 3. MoD Agreement NNR/2042/1. 65pp.

Li, J.-G. and Atkinson, B. W. 1998b. *Numerical Modelling of the Propagation Environment in the Atmospheric Boundary Layer Over Coastal Areas: Real Case Study — The Persian Gulf.* Tech. Rept. 4. MoD Agreement NNR/2042/1. 42pp.

Mulhearn, P. J. 1981. On the Formation of a Stably Stratified Internal Boundary Layer by Advection of Warm Air over a Cooler Sea. *Bound. Lay. Meteorol.*, **21**, 247–254.

Nieuwstadt, F. T. M. 1984. The Turbulent Structure of the Stable Nocturnal Boundary Layer. *J. Atmos. Sci.*, **41**, 2202–2216.

Nieuwstadt, F. T. M. and Tennekes, H. 1981. A Rate Equation for the Nocturnal Boundary Layer Height. *J. Atmos. Sci.*, **38**, 1418–1428.

Physick, W. L., Abbs, D. J. and Pielke, R. A. 1989. Formulation of the Thermal Internal Boundary Layer in a Mesoscale Model. *Bound. Lay. Meteorol.*, **49**, 99–111.

Plant, R. S. and Atkinson, B. W. 1999. *Numerical Modelling of the Propagation Environment in the Atmospheric Boundary Layer of Littoral Areas*

— *Resolution Effects.* Tech. Rept. 1. MoD Agreement FS2/2042/02. 61pp.

Raynor, G. S., Michael, P., Brown, R. M. and SethuRaman, S. 1975. Studies of Atmospheric Diffusion from a Nearshore Oceanic Site. *J. Appl. Meteorol.*, **14**, 1080–1094.

Stull, R. B. 1988. *An Introduction to Boundary Layer Meteorology.* Kluwer Academic Publishers. 666pp.

Stunder, M. and SethuRaman, S. 1985. A Comparative Evaluation of the Coastal Internal Boundary–Layer Height Equations. *Bound. Lay. Meteorol.*, **32**, 177–204.

Tables

Table 1: Initial conditions specified for the numerical simulations in the high wind case. θ denotes the potential temperature and RH the relative humidity.

Level	Height (m)	Pressure (mb)	θ (C)	Temperature (C)	RH (%)
0	0.0	1013.25	22.50	22.50	75.00
1	10.0	1012.14	22.65	22.55	73.00
2	20.0	1011.04	22.80	22.60	71.00
3	30.0	1009.94	22.95	22.65	69.00
4	40.0	1008.83	23.10	22.70	67.00
5	50.0	1007.74	23.25	22.75	65.00
6	60.0	1006.64	23.40	22.80	63.00
7	70.0	1005.54	23.55	22.85	61.00
8	80.0	1004.44	23.70	22.90	59.00
9	90.0	1003.35	23.85	22.95	57.00
10	100.0	1002.26	24.00	23.00	55.00
11	110.0	1001.17	24.12	23.02	53.00
12	120.0	1000.08	24.24	23.04	51.00
13	130.0	998.99	24.36	23.06	49.00
14	140.0	997.90	24.48	23.08	47.00
15	150.0	996.81	24.60	23.10	45.00
16	160.0	995.73	24.72	23.12	43.00
17	180.0	993.56	24.96	23.15	39.00
18	200.0	991.40	25.20	23.19	35.00
19	220.0	989.25	25.44	23.23	31.00
20	240.0	987.10	25.68	23.27	27.00
21	260.0	984.95	25.92	23.31	23.00
22	280.0	982.81	26.16	23.34	19.00
23	300.0	980.68	26.40	23.38	15.00
24	350.0	975.36	27.00	23.47	14.95
25	400.0	970.08	27.60	23.57	14.90
26	450.0	964.83	28.20	23.66	14.85
27	500.0	959.61	28.80	23.75	14.80
28	600.0	949.26	30.00	23.92	14.70
29	800.0	928.56	31.00	22.89	14.50
30	1000.0	908.18	32.00	21.87	14.30
31	1300.0	878.18	33.50	20.33	14.00
32	1600.0	848.87	35.00	18.79	13.70
33	1900.0	820.24	36.50	17.26	13.40
34	2200.0	792.30	38.00	15.72	13.10
35	2600.0	756.08	40.00	13.68	12.70

Continued on next page

Table 1 – continued from previous page

Level	Height (m)	Pressure (mb)	θ (C)	Temperature (C)	RH (%)
36	3000.0	721.03	42.00	11.64	12.30
37	3500.0	678.85	44.50	9.09	11.80
38	4000.0	638.43	47.00	6.55	11.30
39	5000.0	562.79	52.00	1.49	10.30
40	6000.0	493.79	57.00	-3.54	9.30
41	8000.0	374.54	67.00	-13.52	7.30

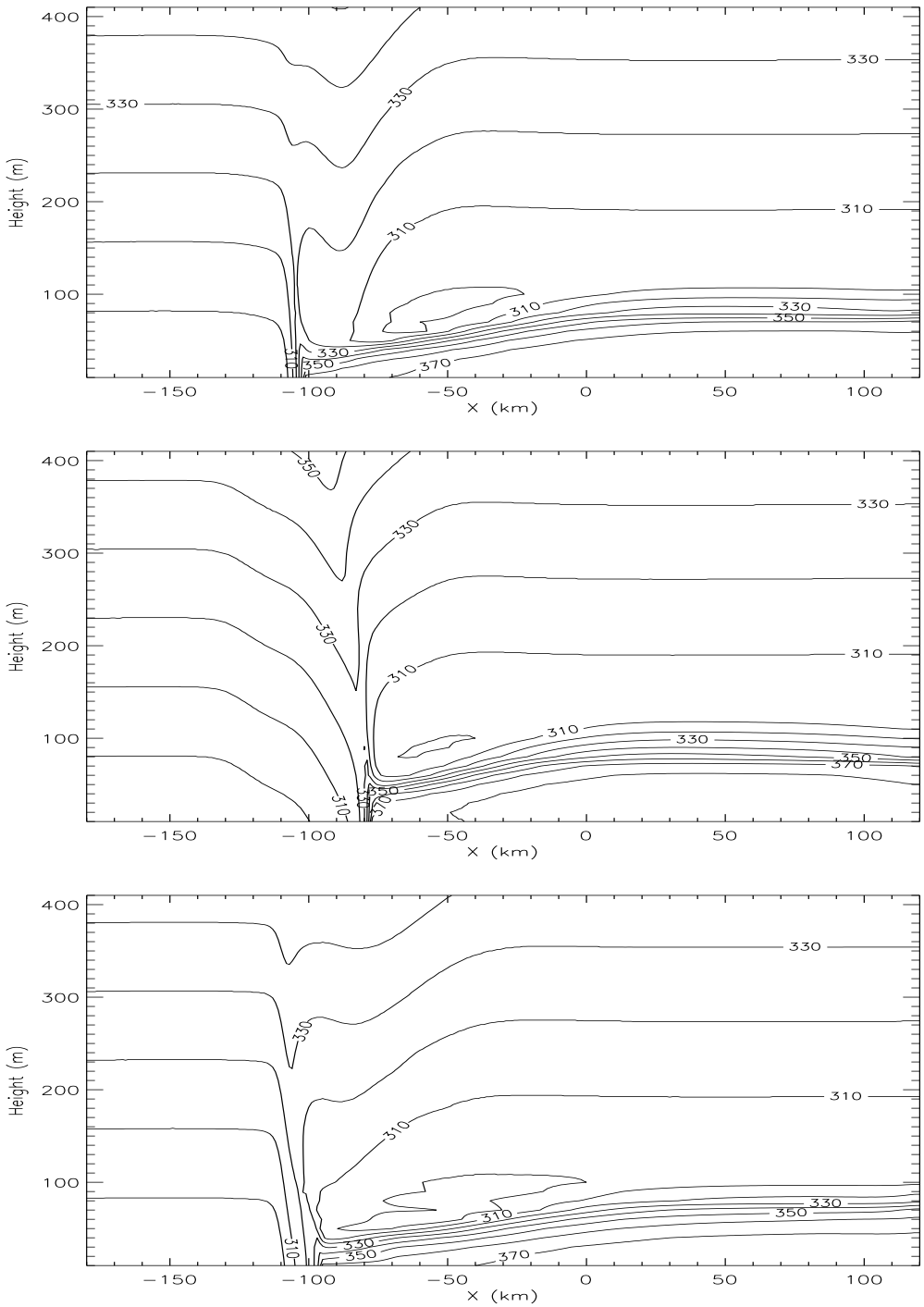

Figure 1: Cross sections of refractivity (M units) at 1500 hr in the low wind case. The plots are obtained from a run with a 1 km grid length. The upper plot is along the line $y = -39$ km, the middle along $y = -54$ km and the lower along $y = -69$ km.

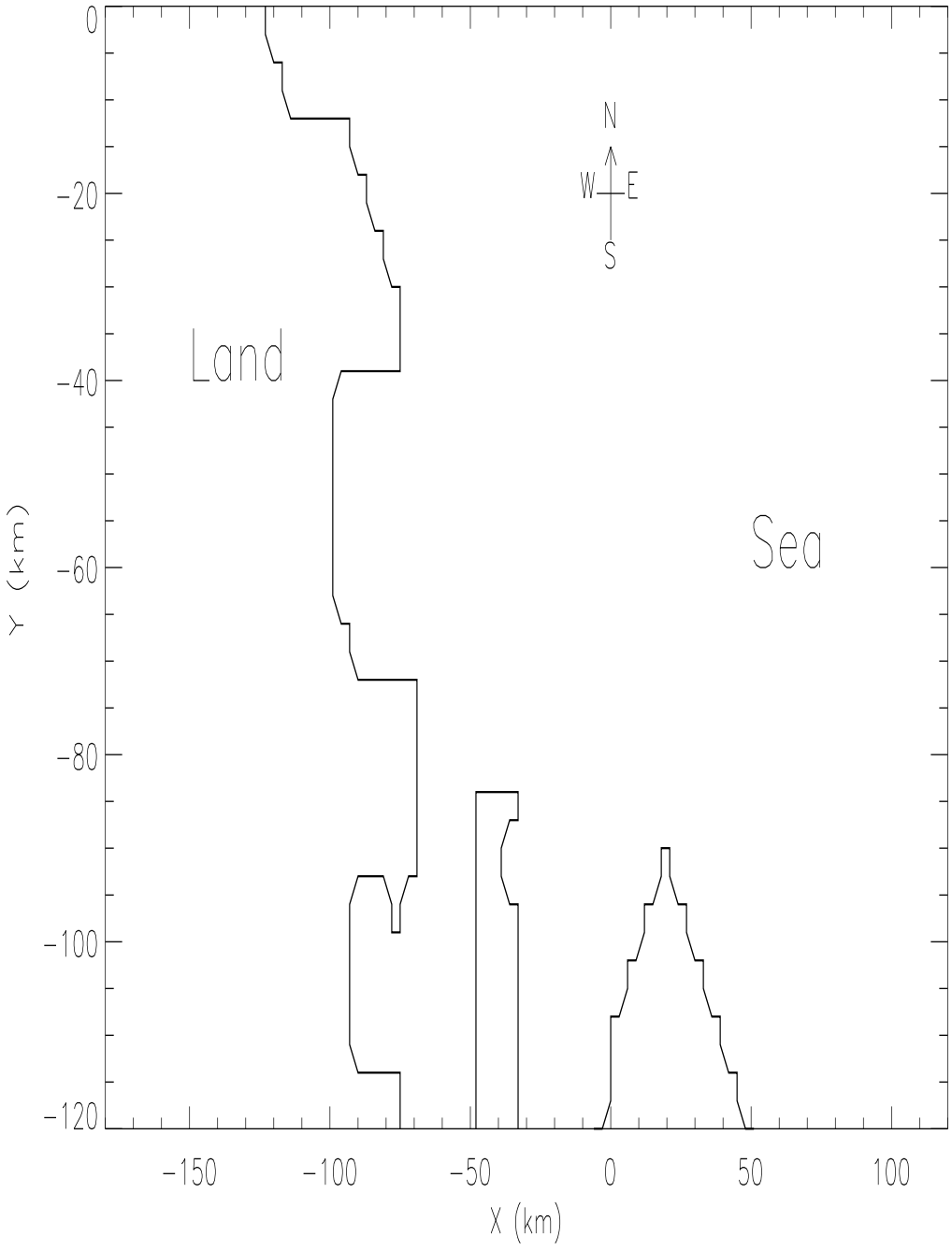

Figure 2: Land and sea areas in the model domain.

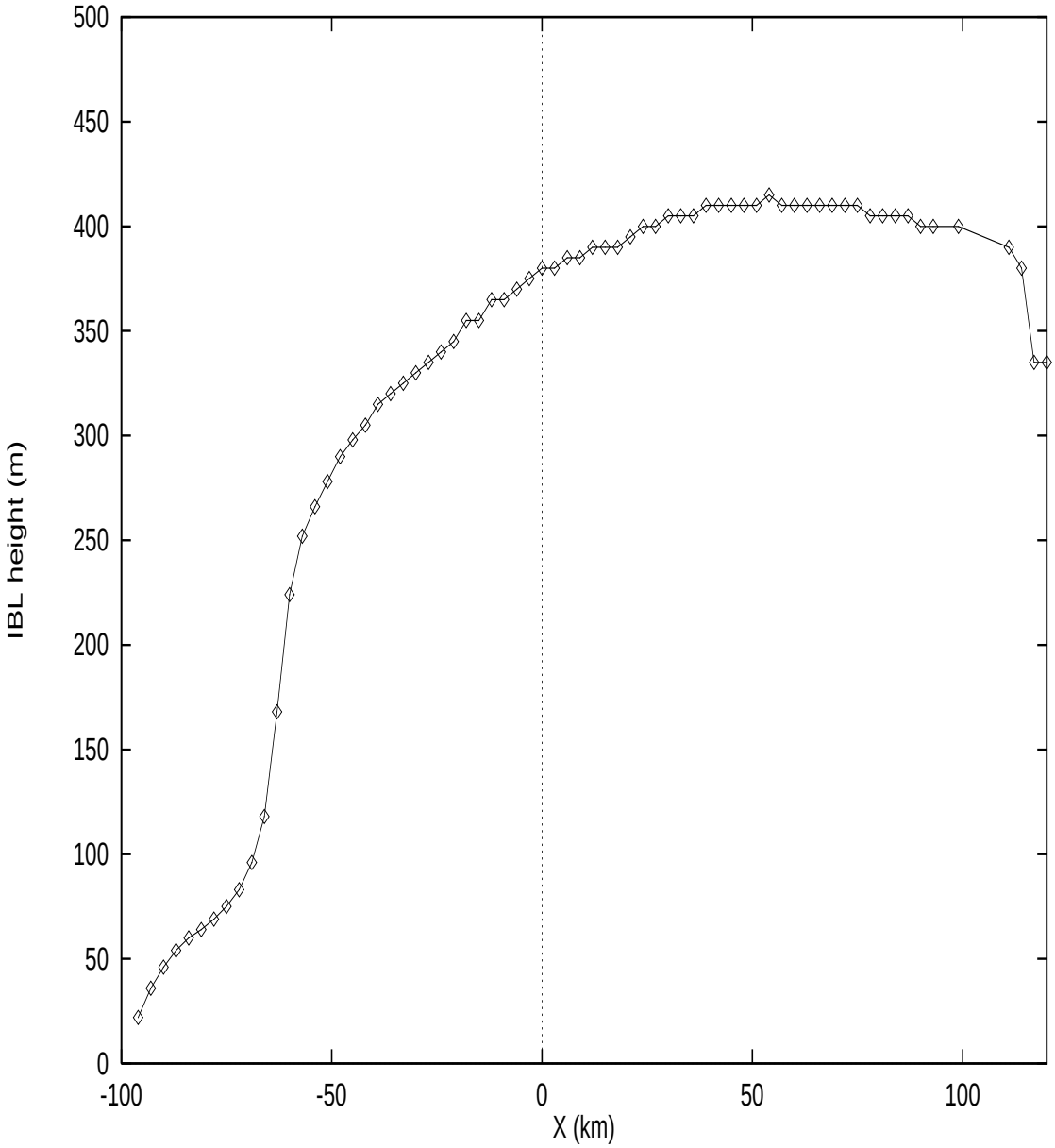

Figure 3: The height of the MIBL is plotted along the line $y = -54$ km at 1500 hr in the high wind case. The height was determined using method 3, as described in Appendix A.

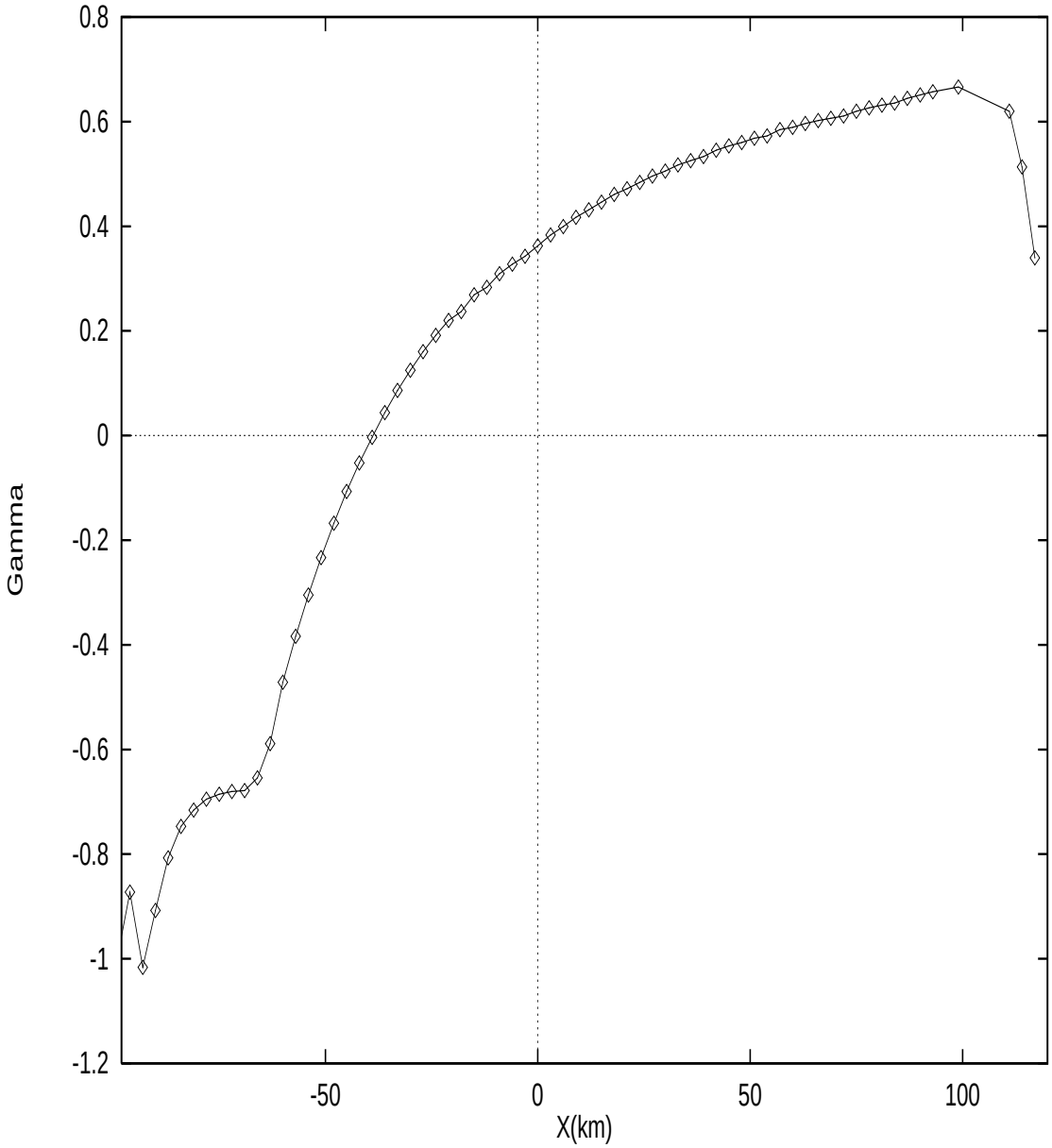

Figure 4: The curvature parameter γ is plotted along the line $y = -54$ km at 1500 hr in the high wind case.

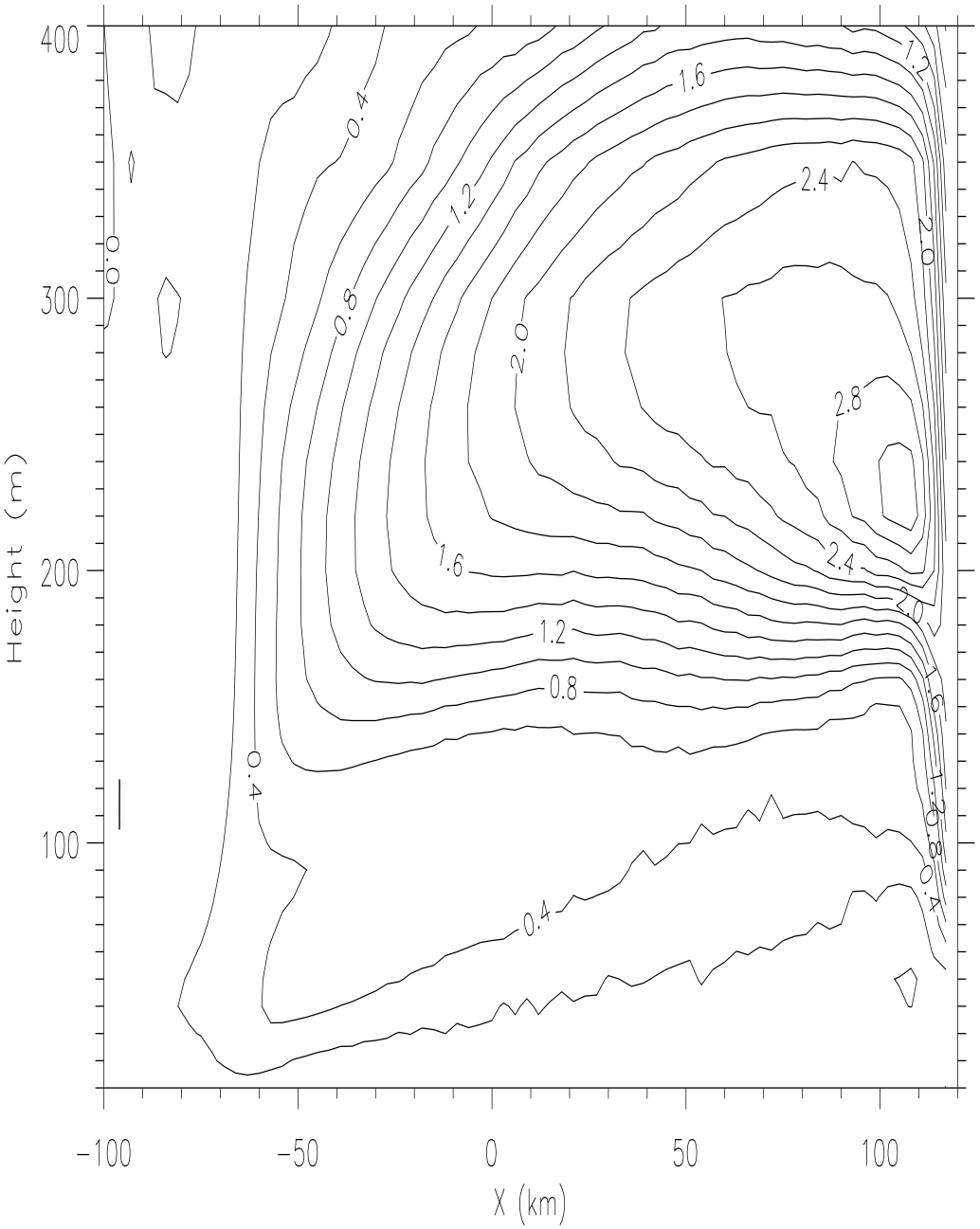

Figure 5: Cross section of the curvature variable n along $y = -54$ km at 1500 hr in the high wind case.

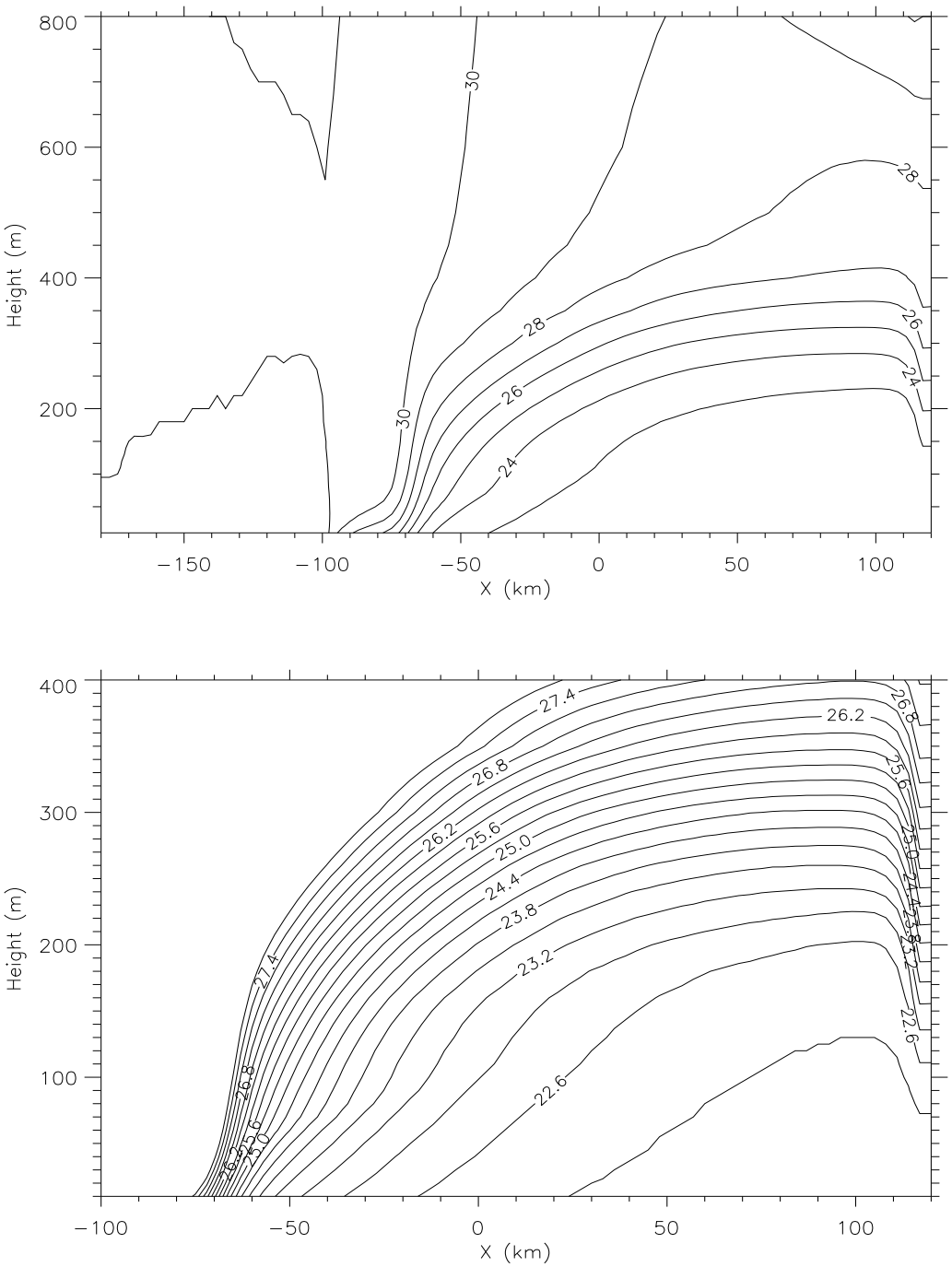

Figure 6: Potential temperature contours along $y = -54$ km at 1500 hr in the high wind case. The upper plot shows contours at 1 K intervals; the lower plot shows contours at 0.3 K intervals, from 22 K to 28 K.

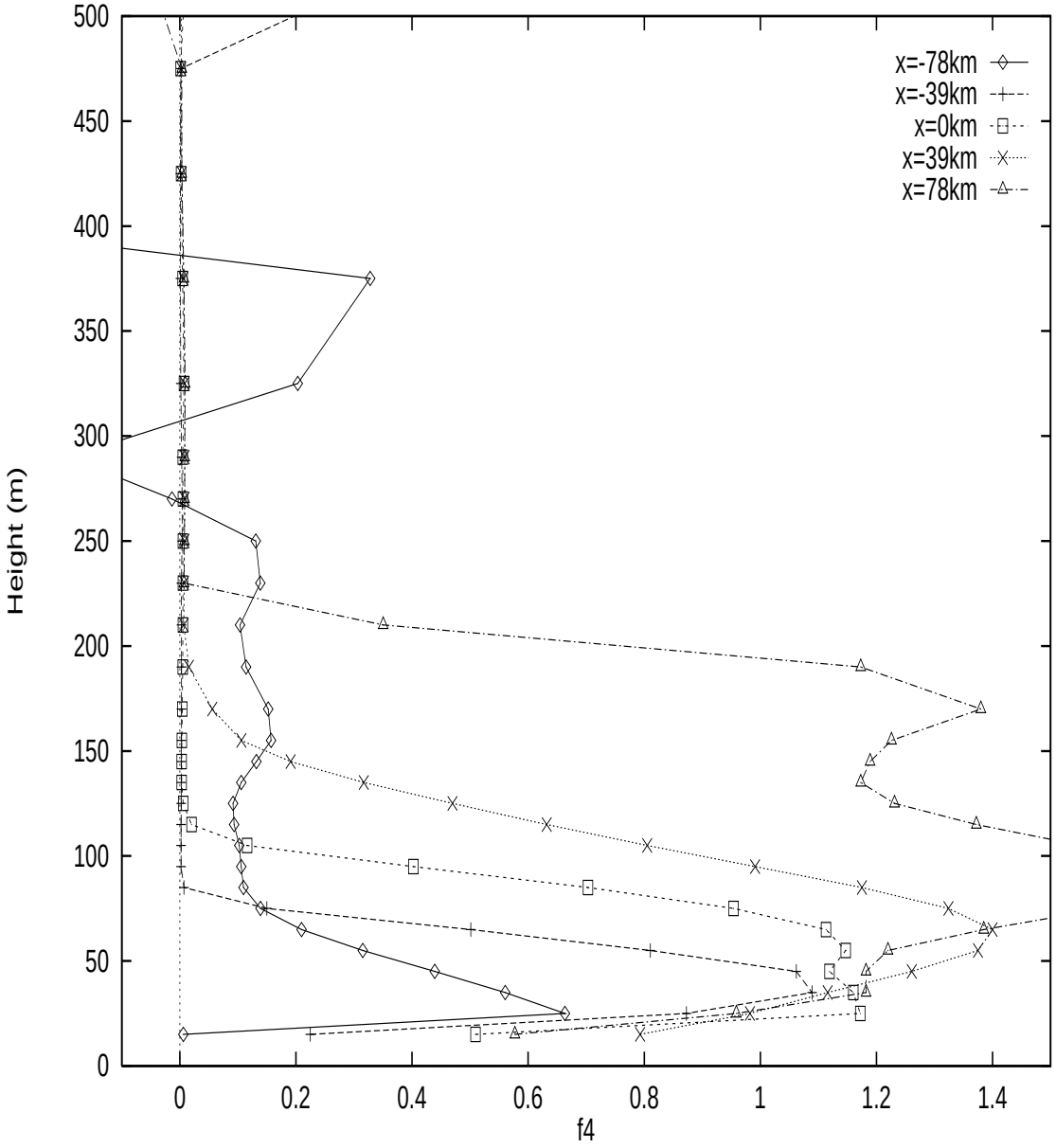

Figure 7: The function f_4 is plotted for various fetches along the line $y = -54$ km at 1500 hr in the high wind case.

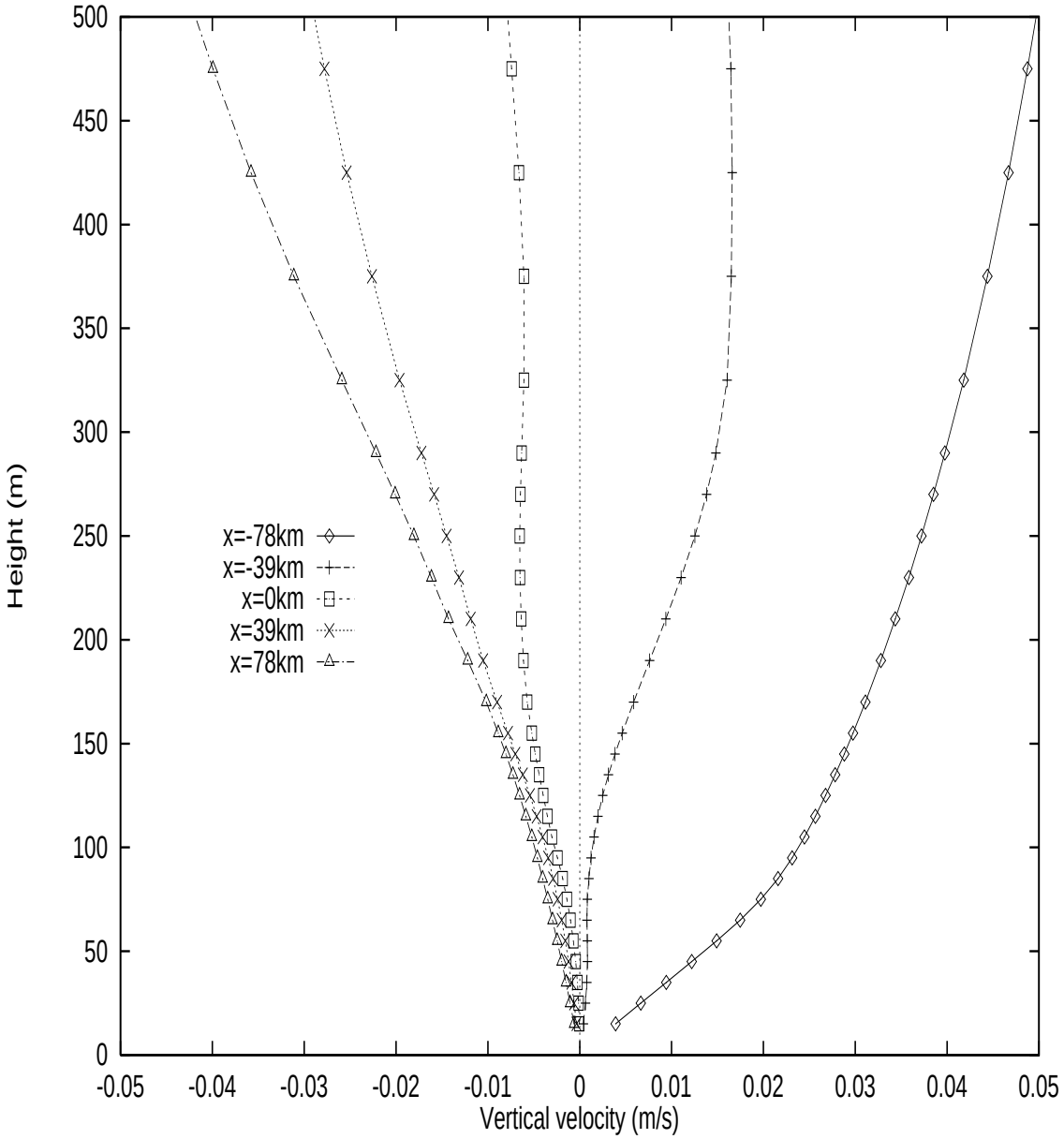

Figure 8: Vertical velocity profiles are plotted for various fetches along the line $y = -54$ km at 1500 hr in the high wind case.

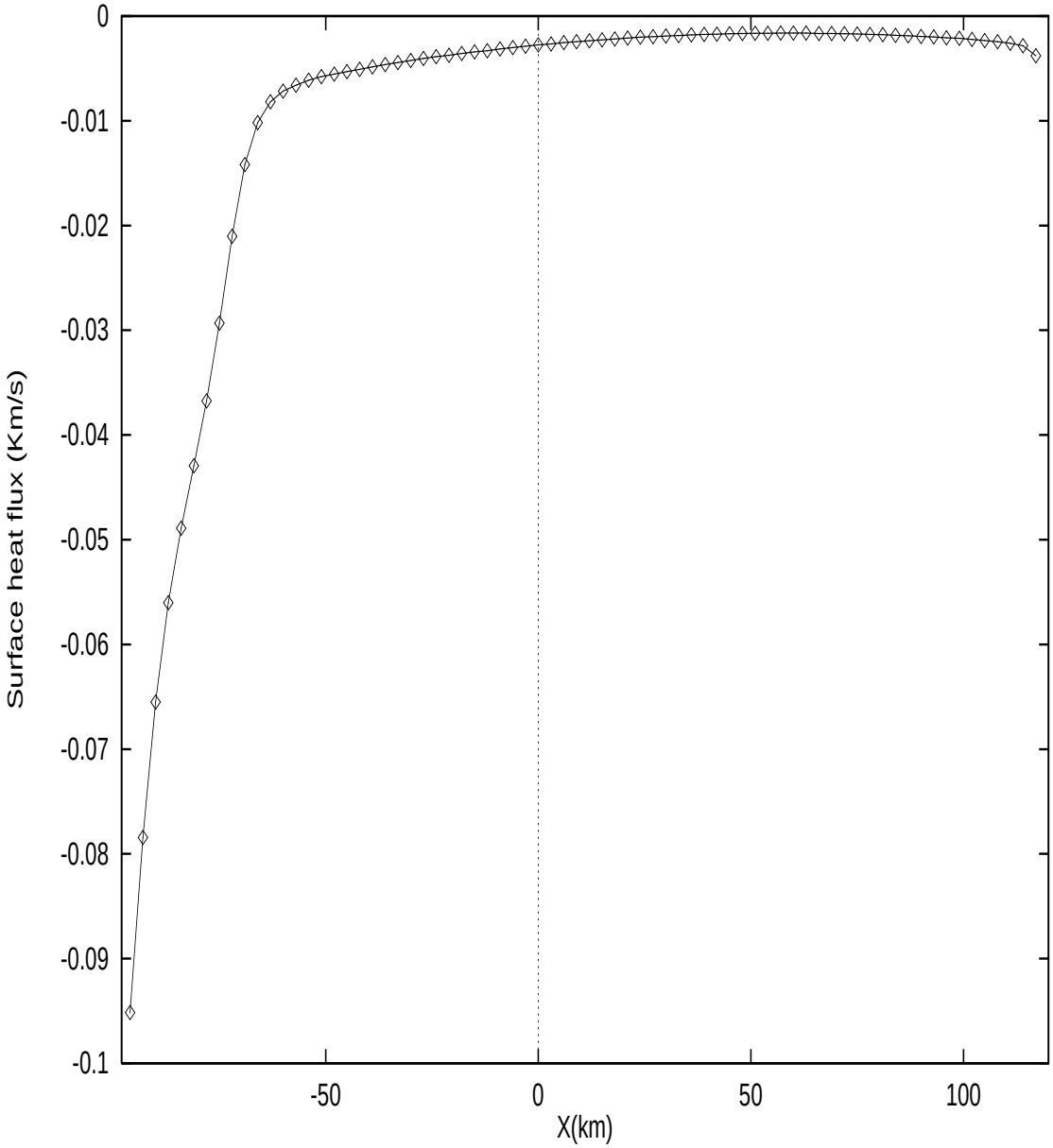

Figure 9: The surface heat flux along the line $y = -54$ km is plotted at 1500 hr in the high wind case.

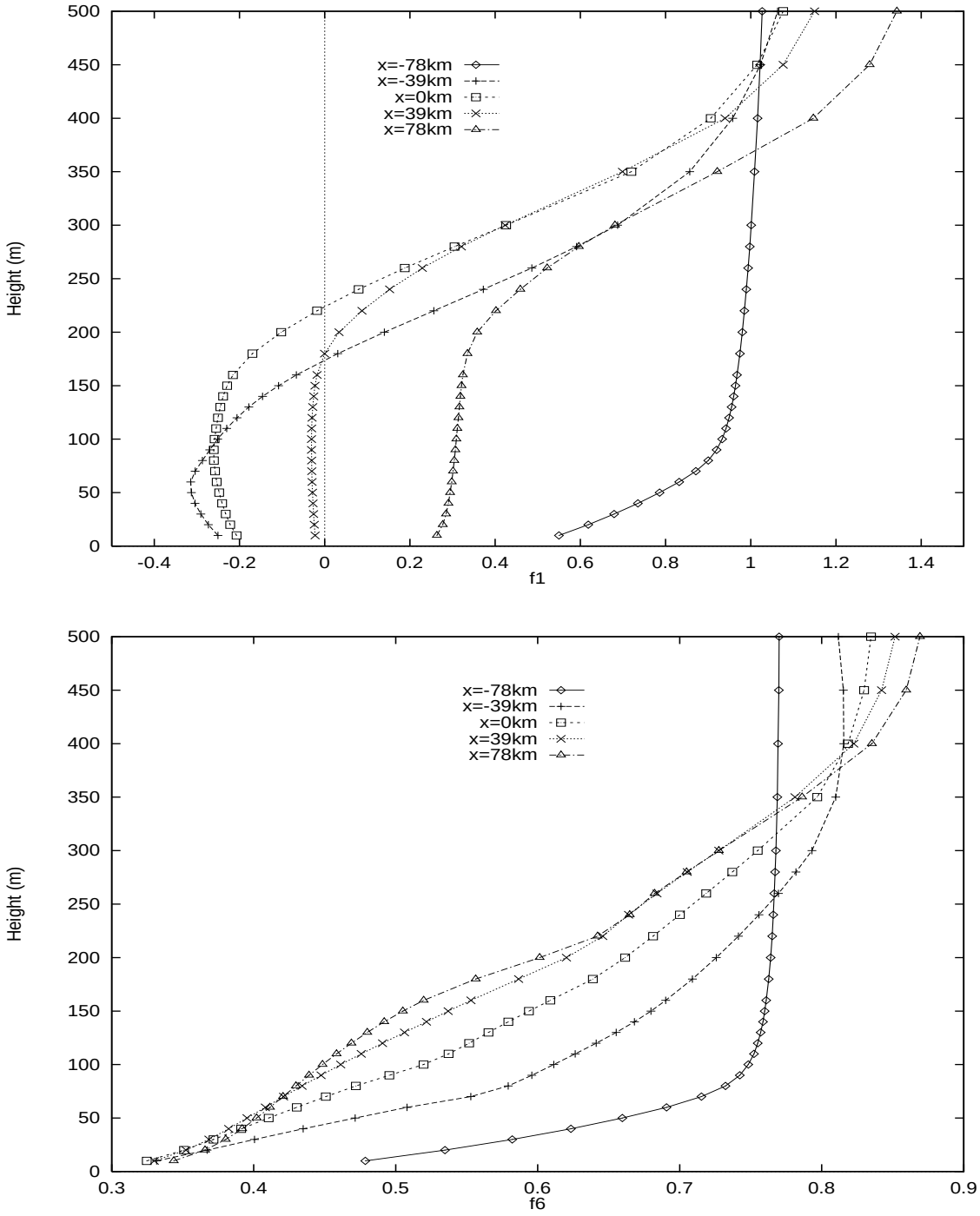

Figure 10: The functions f_1 and f_6 are plotted for various fetches along the line $y = -54$ km at 1500 hr in the high wind case. The upper plot shows f_1; the lower plot shows f_6.

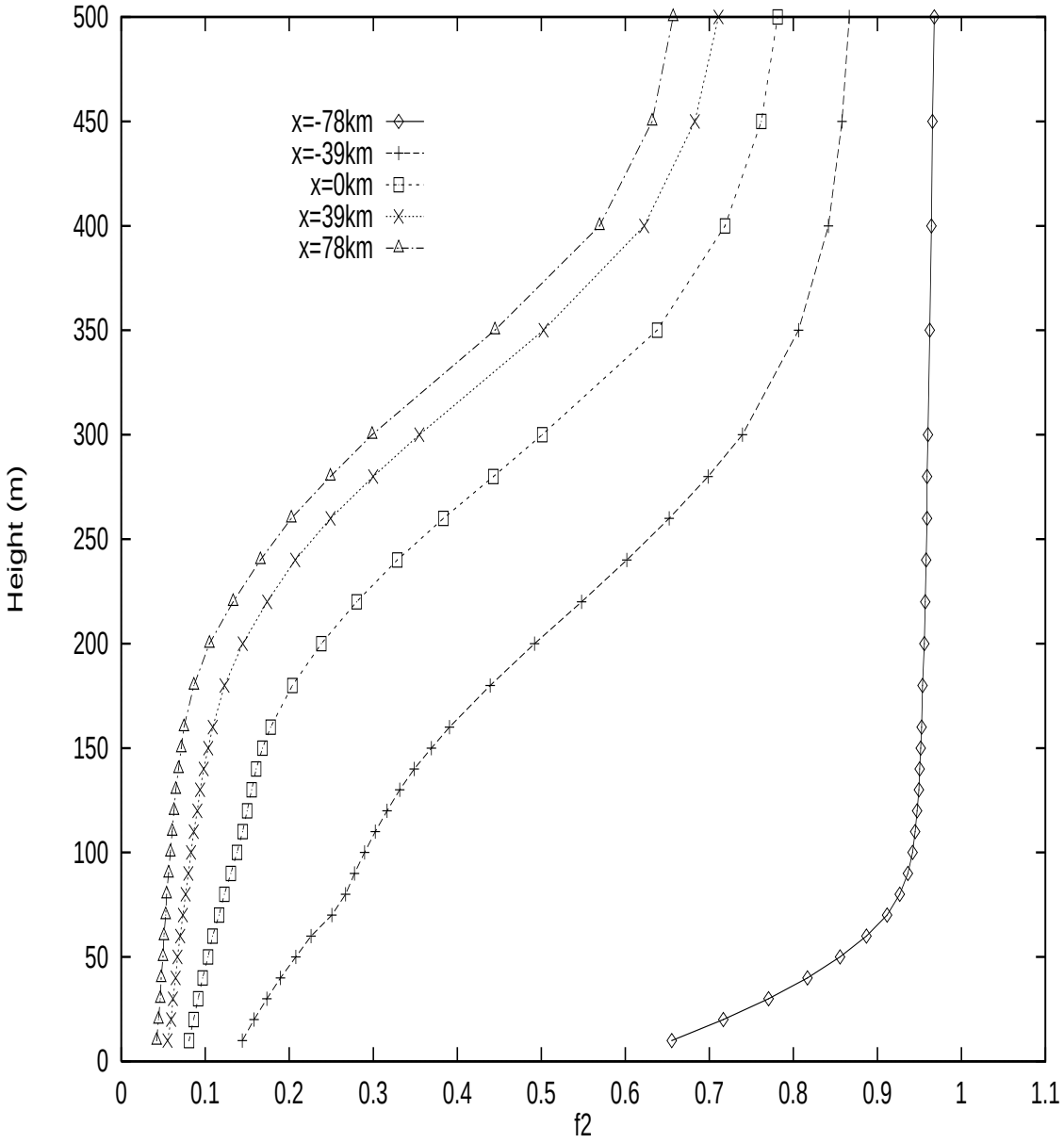

Figure 11: The function f_2 is plotted for various fetches along the line $y = -54$ km at 1500 hr in the high wind case.

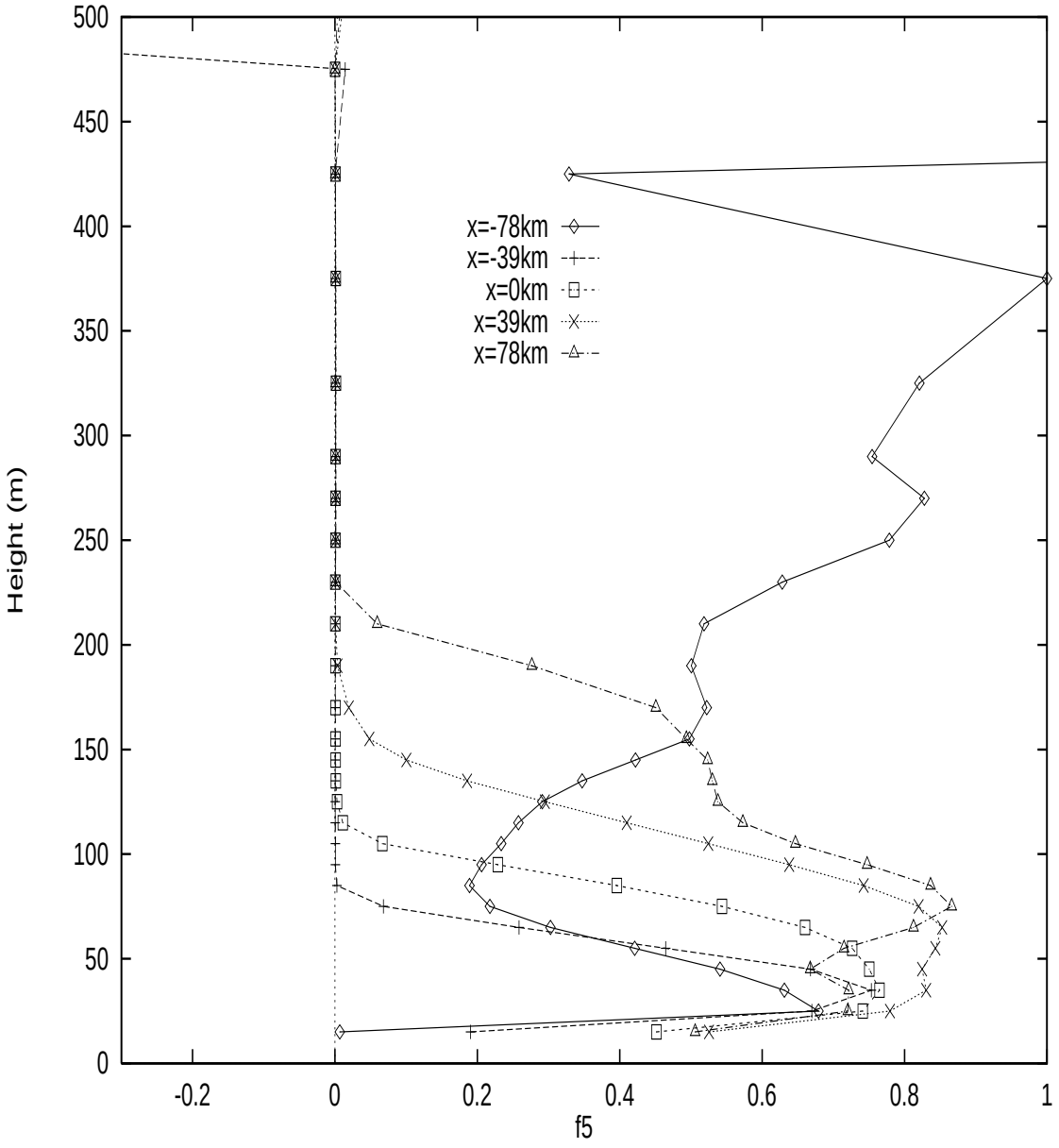

Figure 12: The function f_5 is plotted for various fetches along the line $y = -54$ km at 1500 hr in the high wind case.

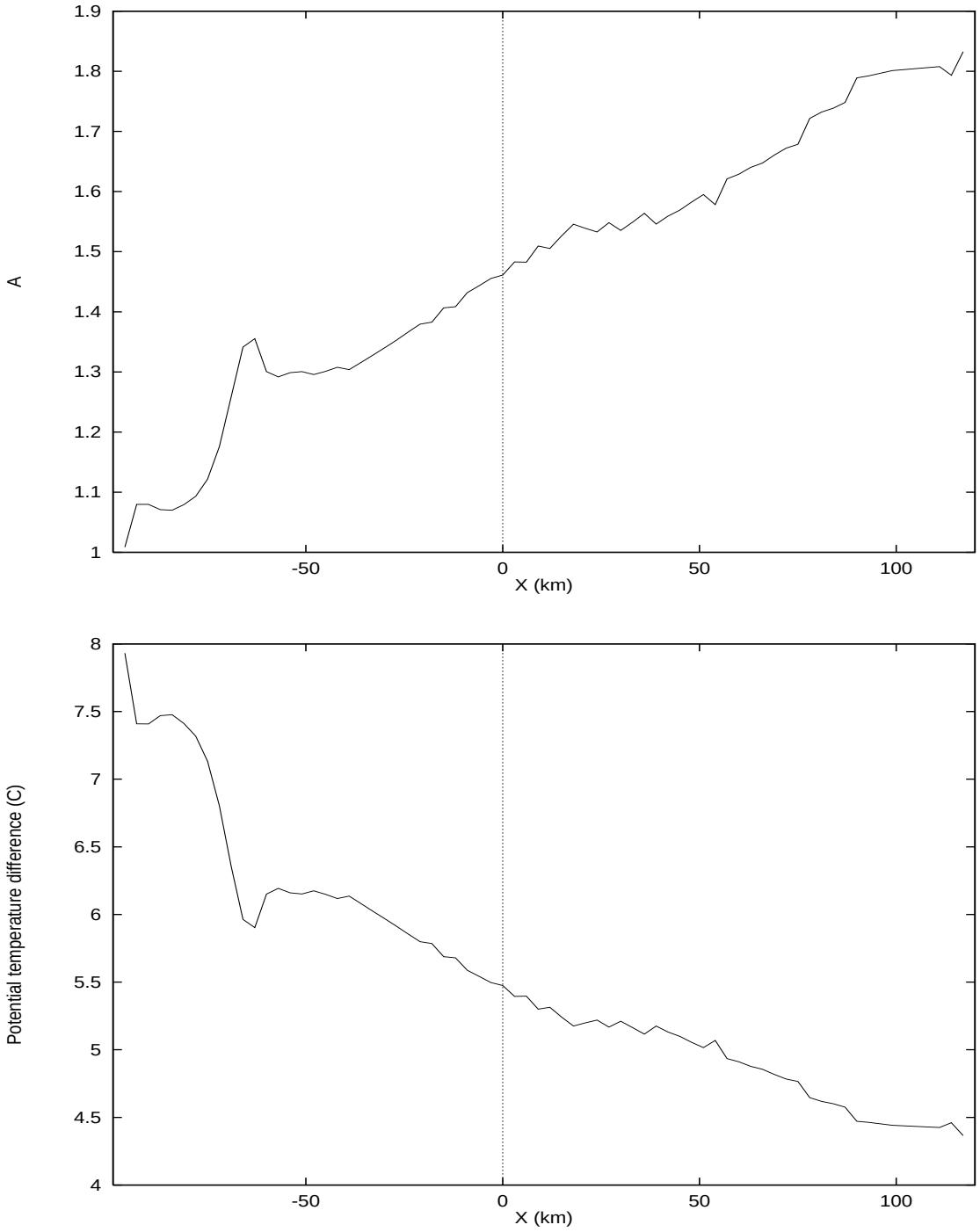

Figure 13: The upper plot shows the parameter A as a function of fetch along the line $y = -54$ km at 1500 hr in the high wind case. The lower plots hows the corresponding potential–temperature difference between the surface and the IBL top.

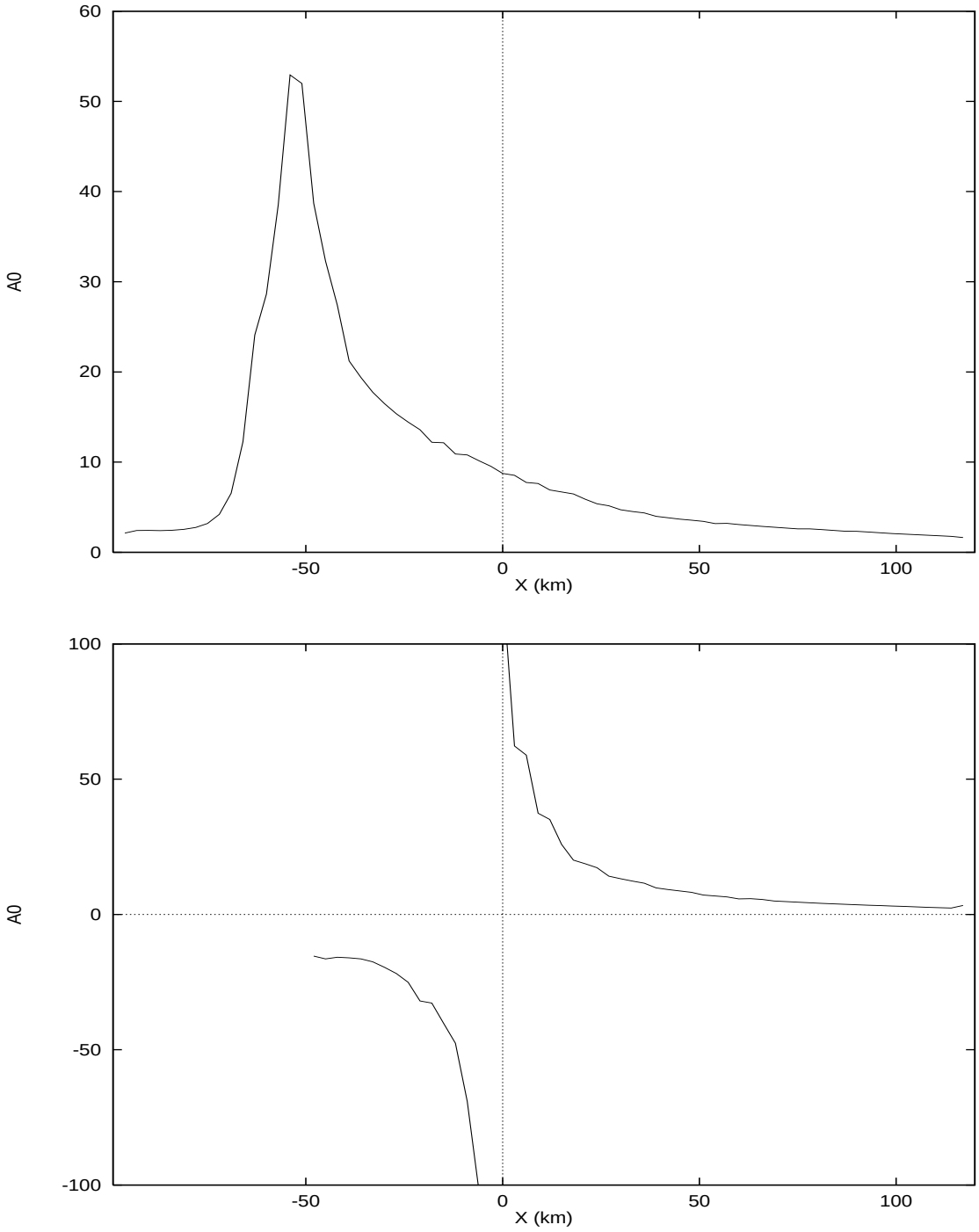

Figure 14: The parameter A_0 is plotted as a function of fetch along the line $y = -54$ km at 1500 hr in the high wind case. In the upper plot, it is evaluated using an IBL height at the top of the inversion; in the lower plot, it is evaluated using an IBL height in the middle of the inversion.

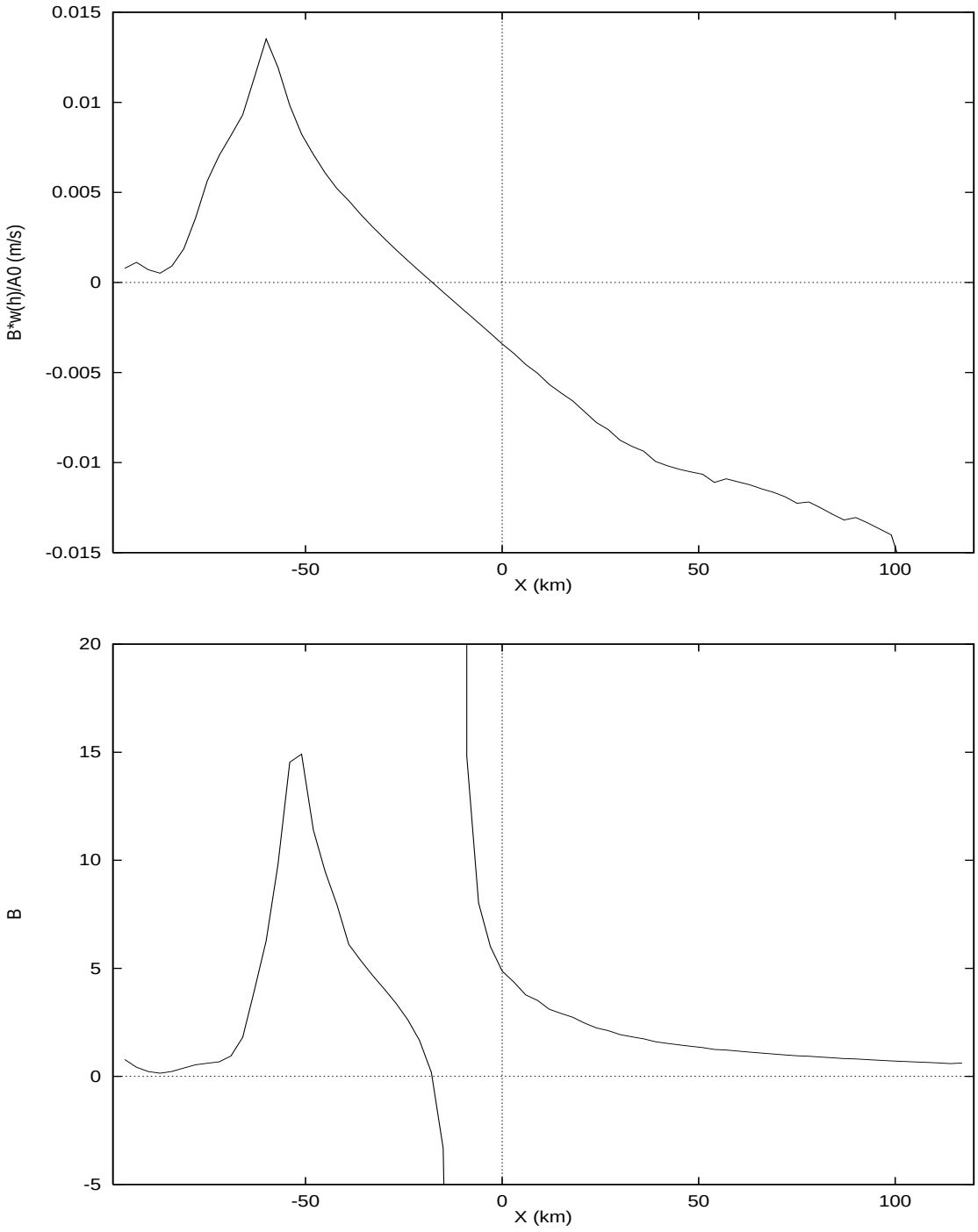

Figure 15: The upper plot shows the combination $Bw(h)/A_0$ as a function of fetch along the line $y = -54$ km at 1500 hr in the high wind case. The lower plot shows the corresponding evolution of parameter B.

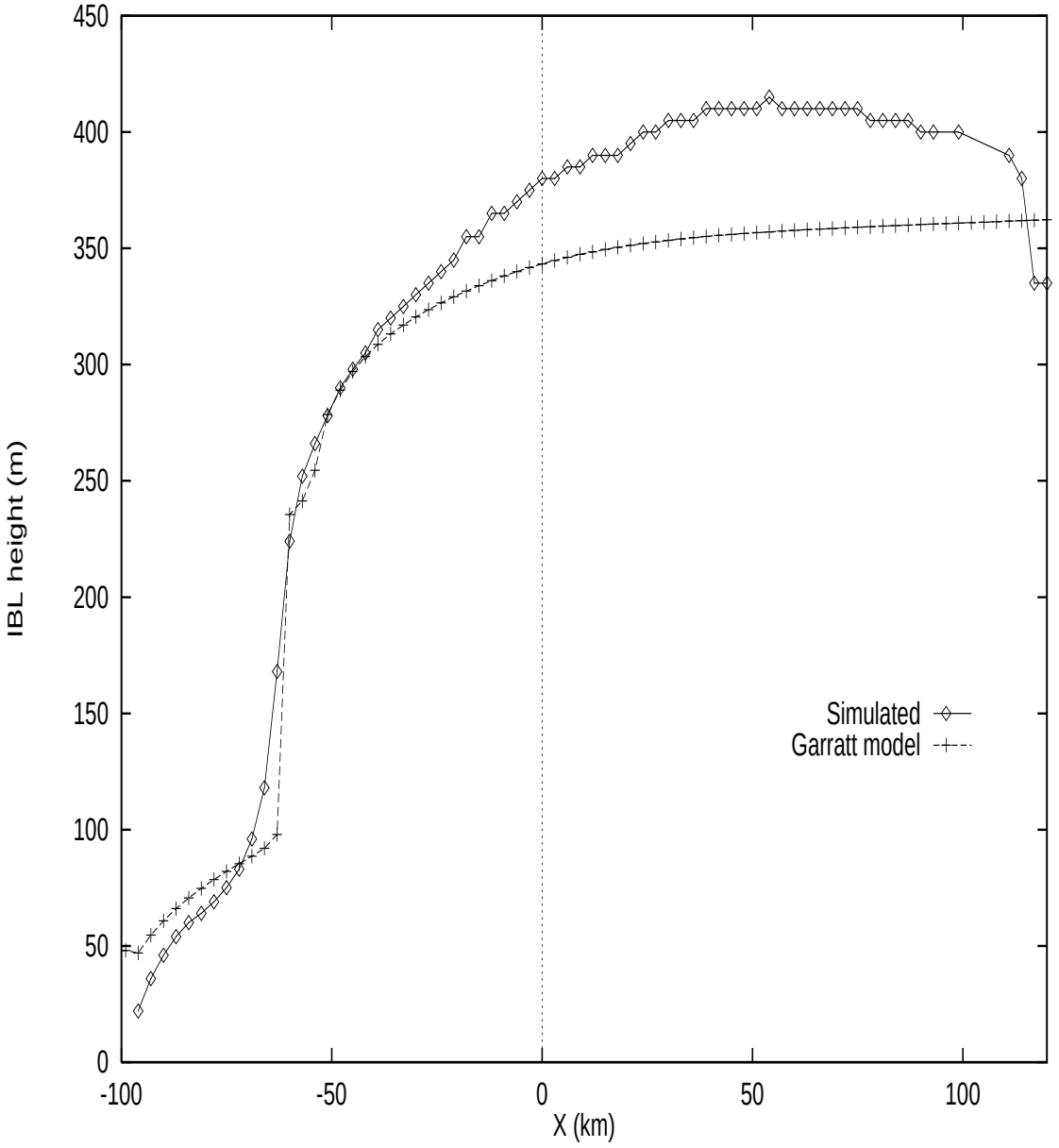

Figure 16: IBL heights predicted from the generalized Garratt model, along the line $y = -54$ km at 1500 hr in the high wind case. A height of 47 m at $x = -96$ km was used as the initial condition. The corresponding simulation results are also shown.

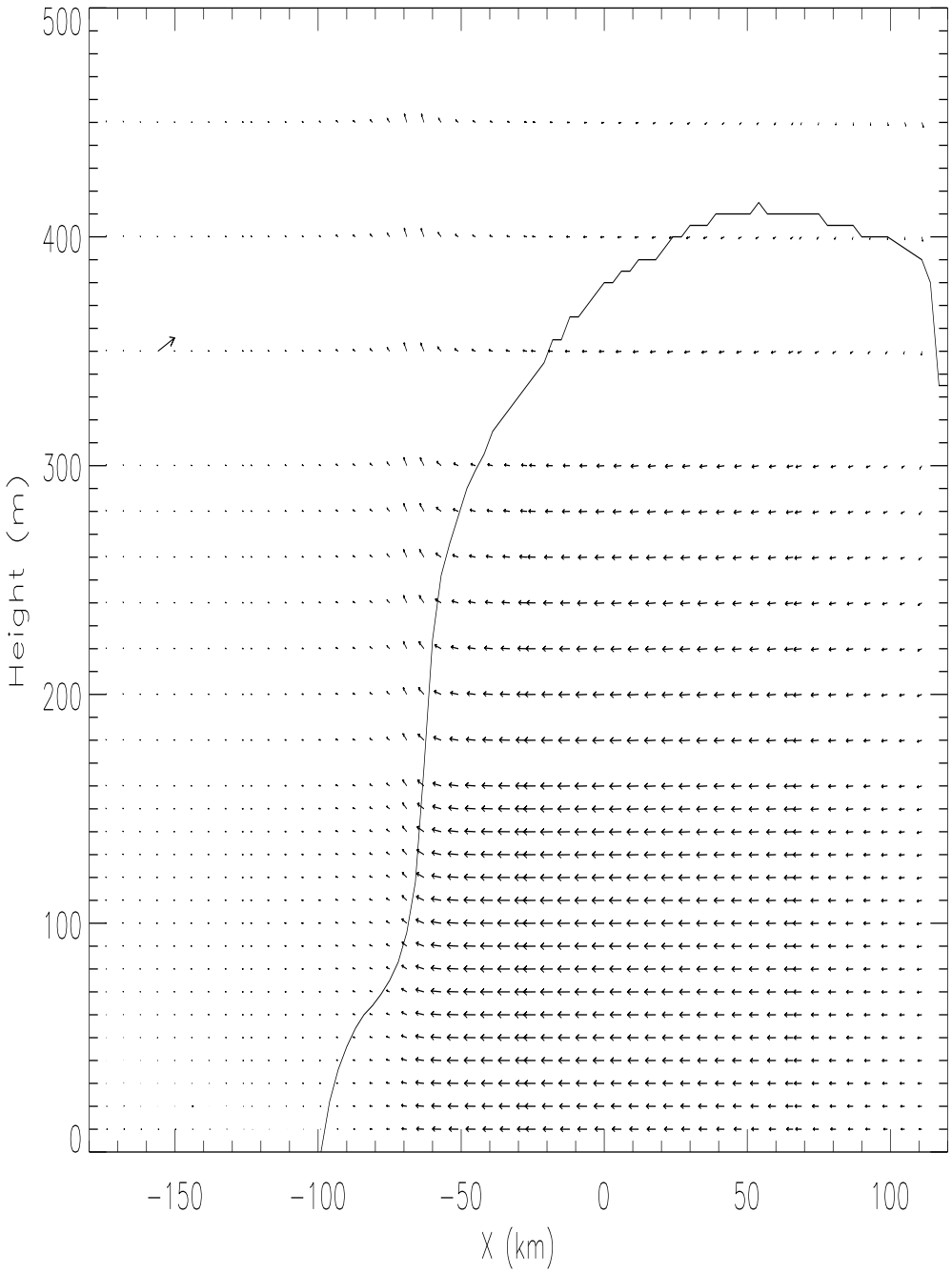

Figure 17: Cross section of the induced wind at 1500 hr along the line $y = -54$ km in the high wind case. The u component of the wind is plotted in units of ms^{-1} and the w component in units of cms^{-1}. Scales are provided by a reference arrow shown at a height of 350 m and $x \sim -150$ km, representing $u = 20$ ms^{-1} and $w = 20$ cms^{-1}. Also plotted is the IBL height.

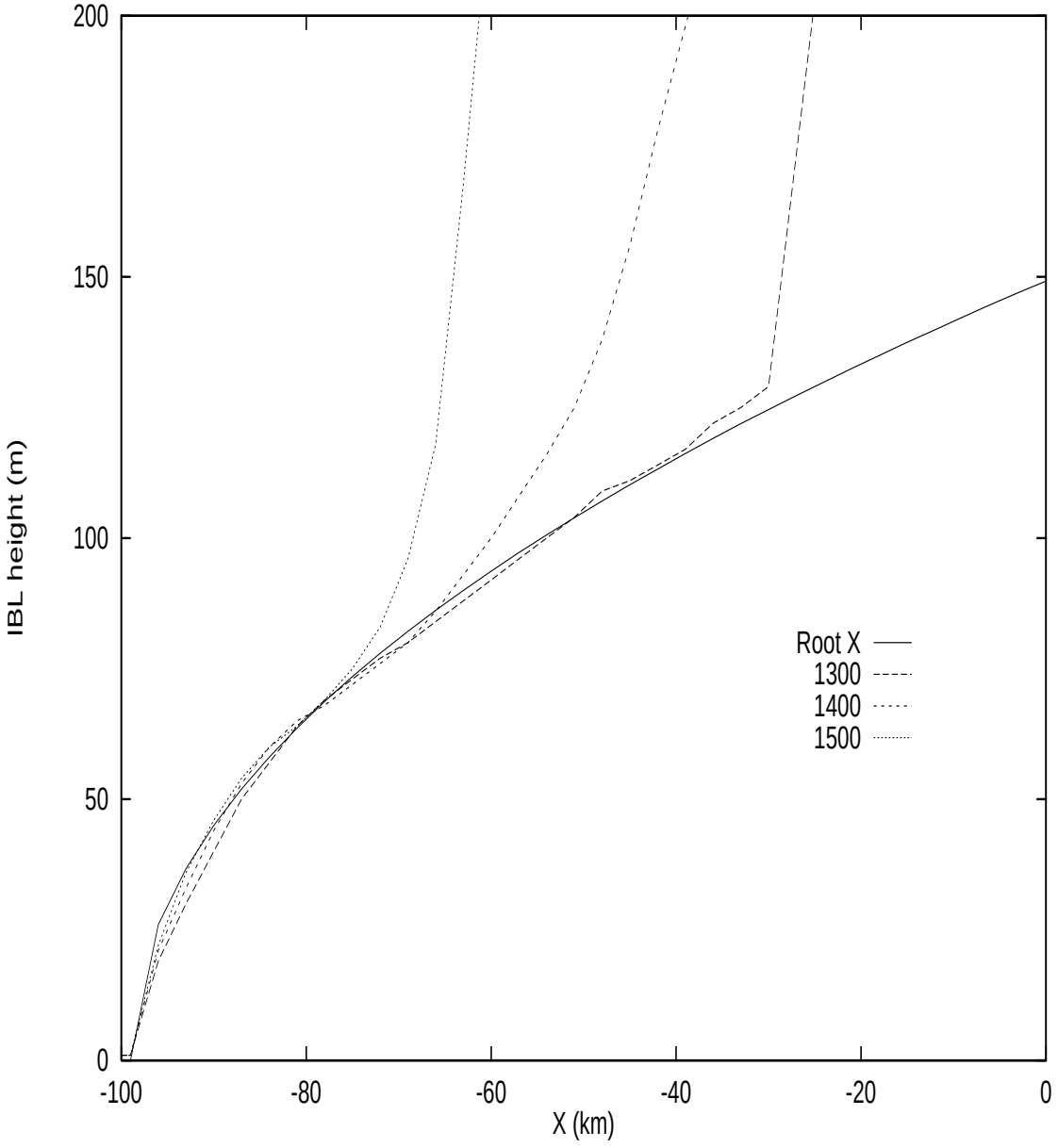

Figure 18: The height of the MIBL is plotted along the line $y = -54$ km in the high wind case. Results are shown at 1300 hr, 1400 hr and 1500 hr. Also shown is the curve $h = a\sqrt{X}$, where X is the distance from the coast in km and $a = 15.0$.

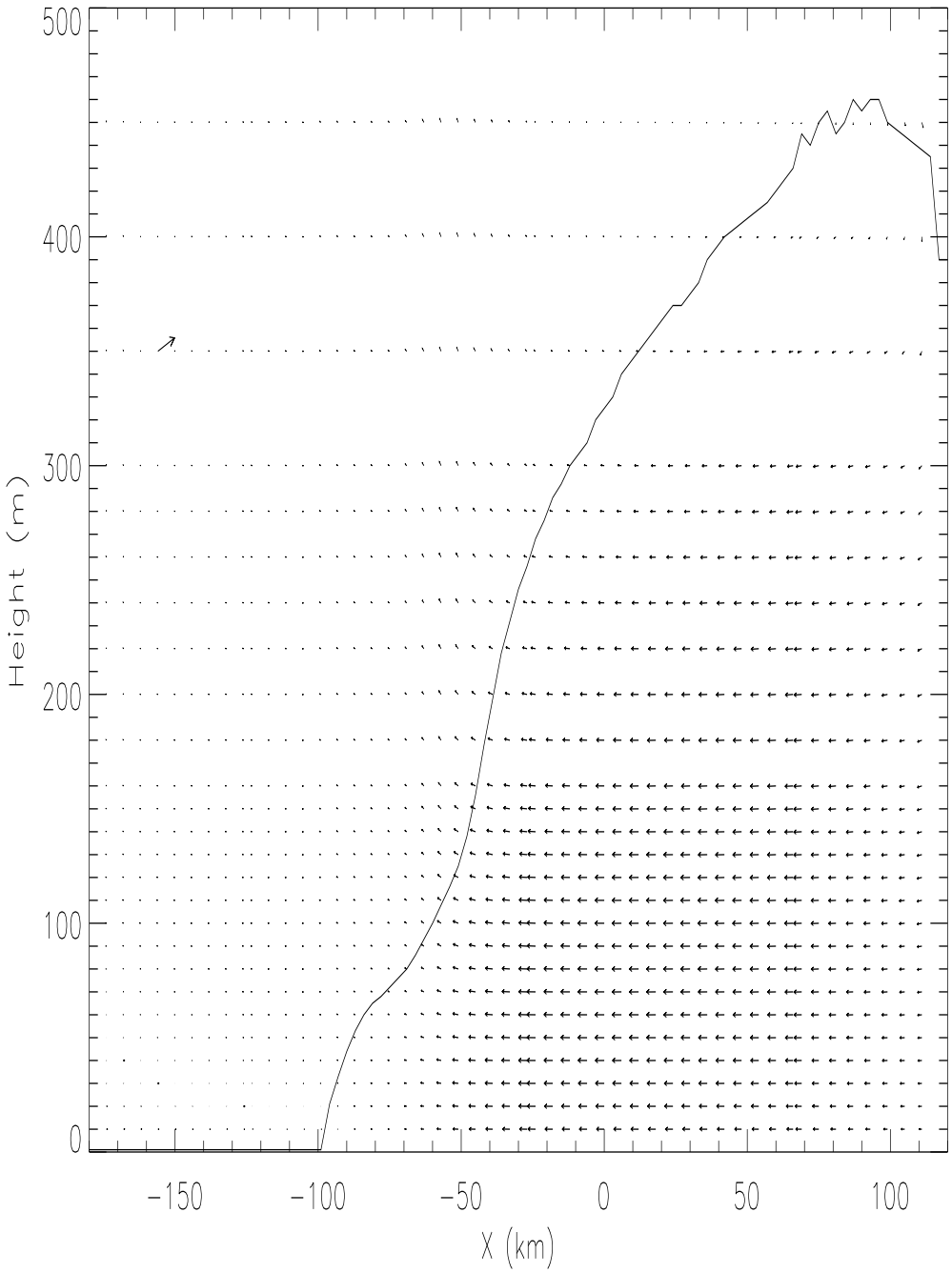

Figure 19: Cross section of the induced wind at 1400 hr along the line $y = -54$ km in the high wind case. The u component of the wind is plotted in units of ms^{-1} and the w component in units of cms^{-1}. Scales are provided by a reference arrow shown at a height of 350 m and $x \sim -150$ km, representing $u = 20$ ms^{-1} and $w = 20$ cms^{-1}. Also plotted is the IBL height.

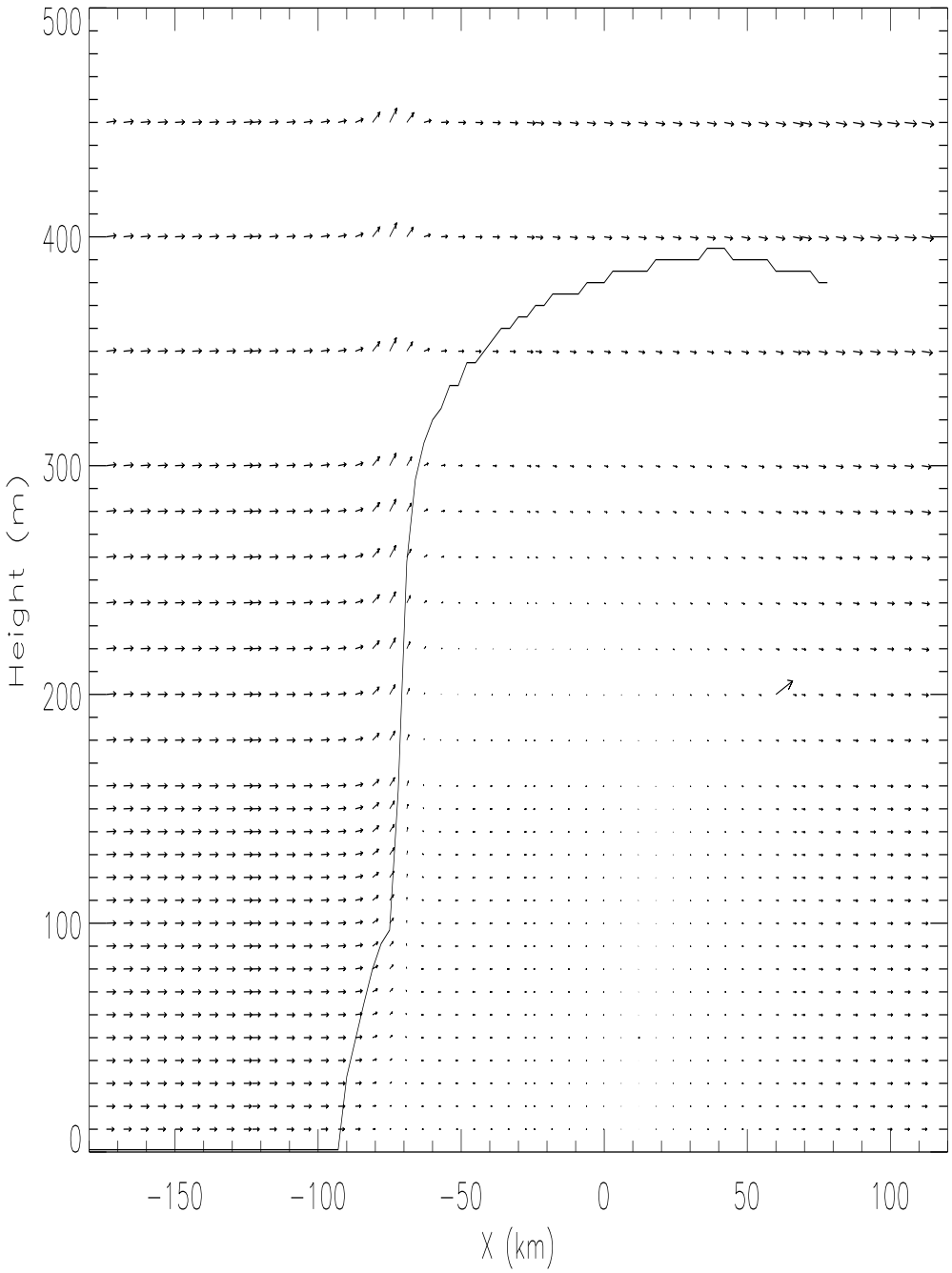

Figure 20: Cross section of the wind at 1600 hr along the line $y = -69$ km in the high wind case. The u component of the wind is plotted in units of ms^{-1} and the w component in units of cms^{-1}. Scales are provided by a reference arrow shown at a height of 200 m and $x \sim 50$ km, representing $u = 20$ ms^{-1} and $w = 20$ cms^{-1}. Also plotted is the IBL height.

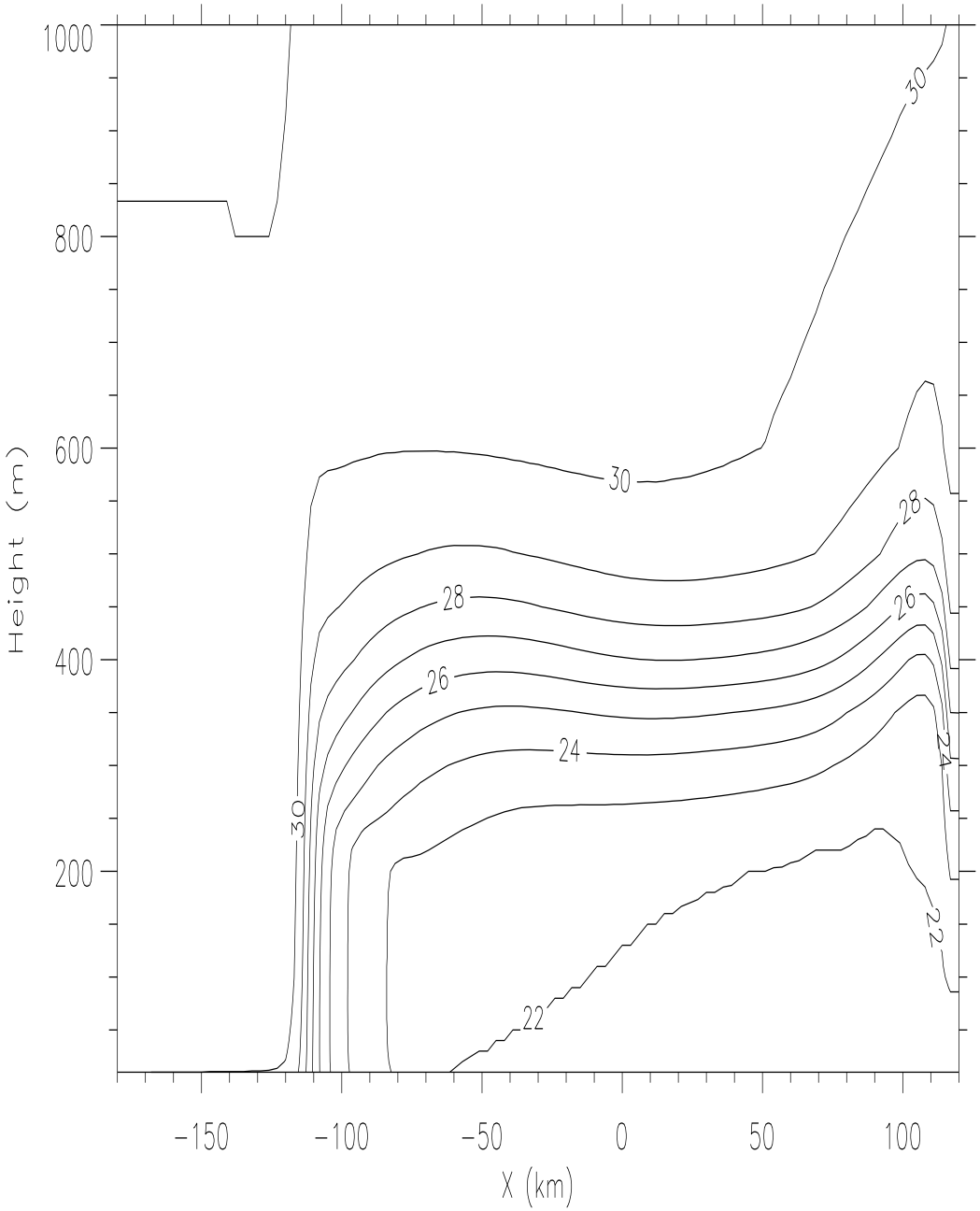

Figure 21: Cross section of potential temperature (C) along $y = -39$ km at 1800 hr in the high wind case.

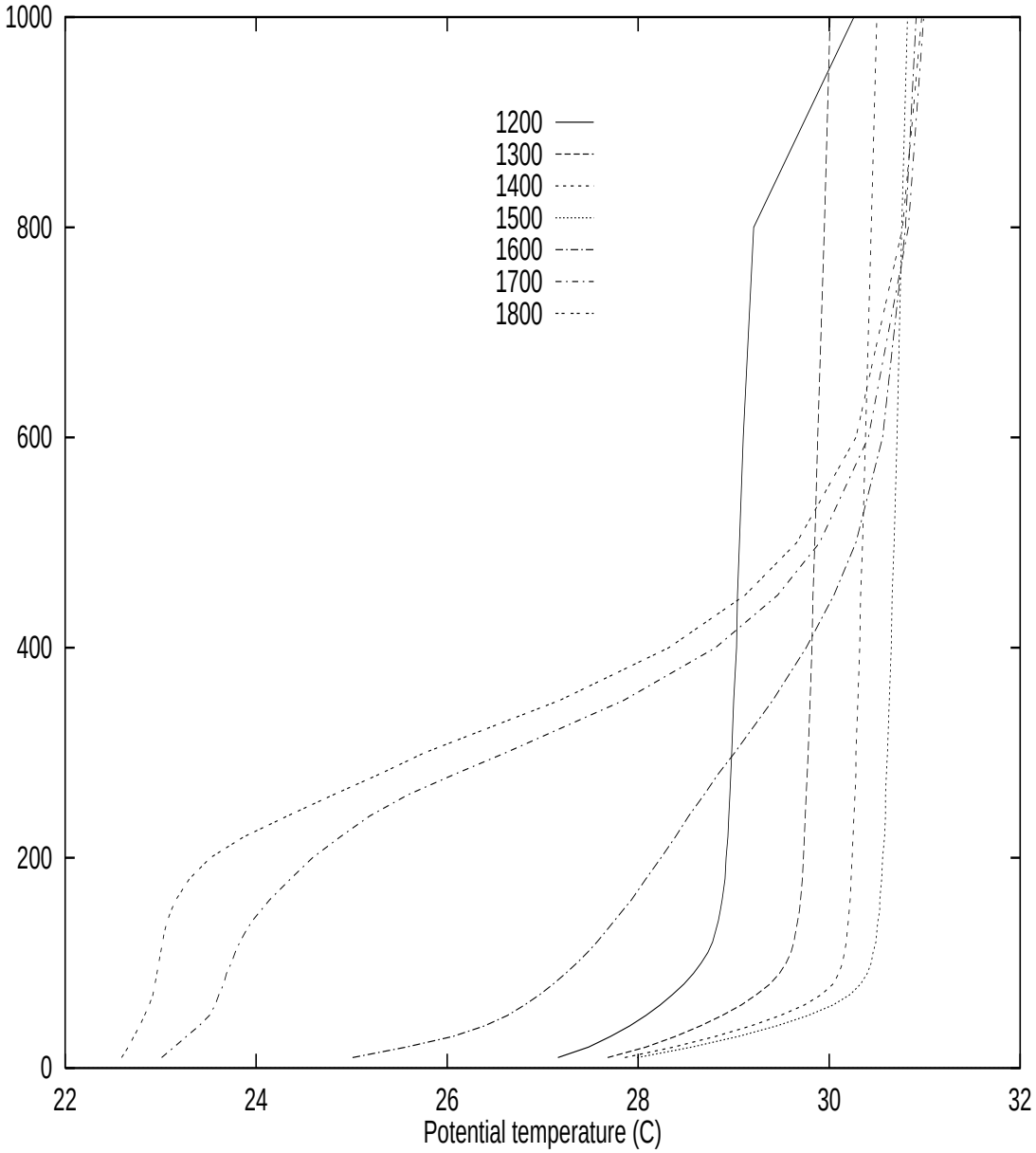

Figure 22: Potential temperature profiles at the point $y = -54$ km, $x = -78$ km in the high wind case.

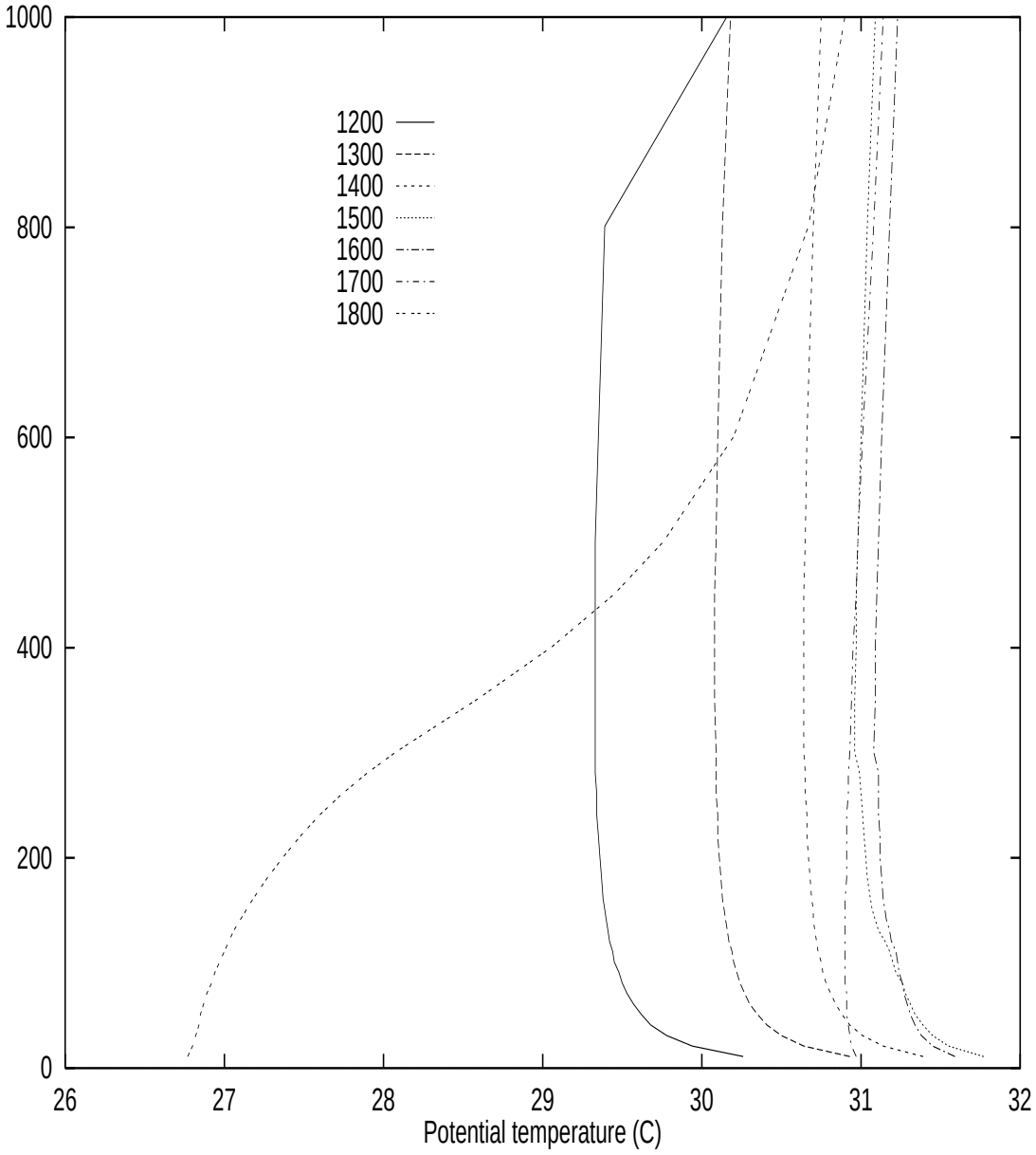

Figure 23: Potential temperature profiles at the point $y = -54$ km, $x = -102$ km in the high wind case.

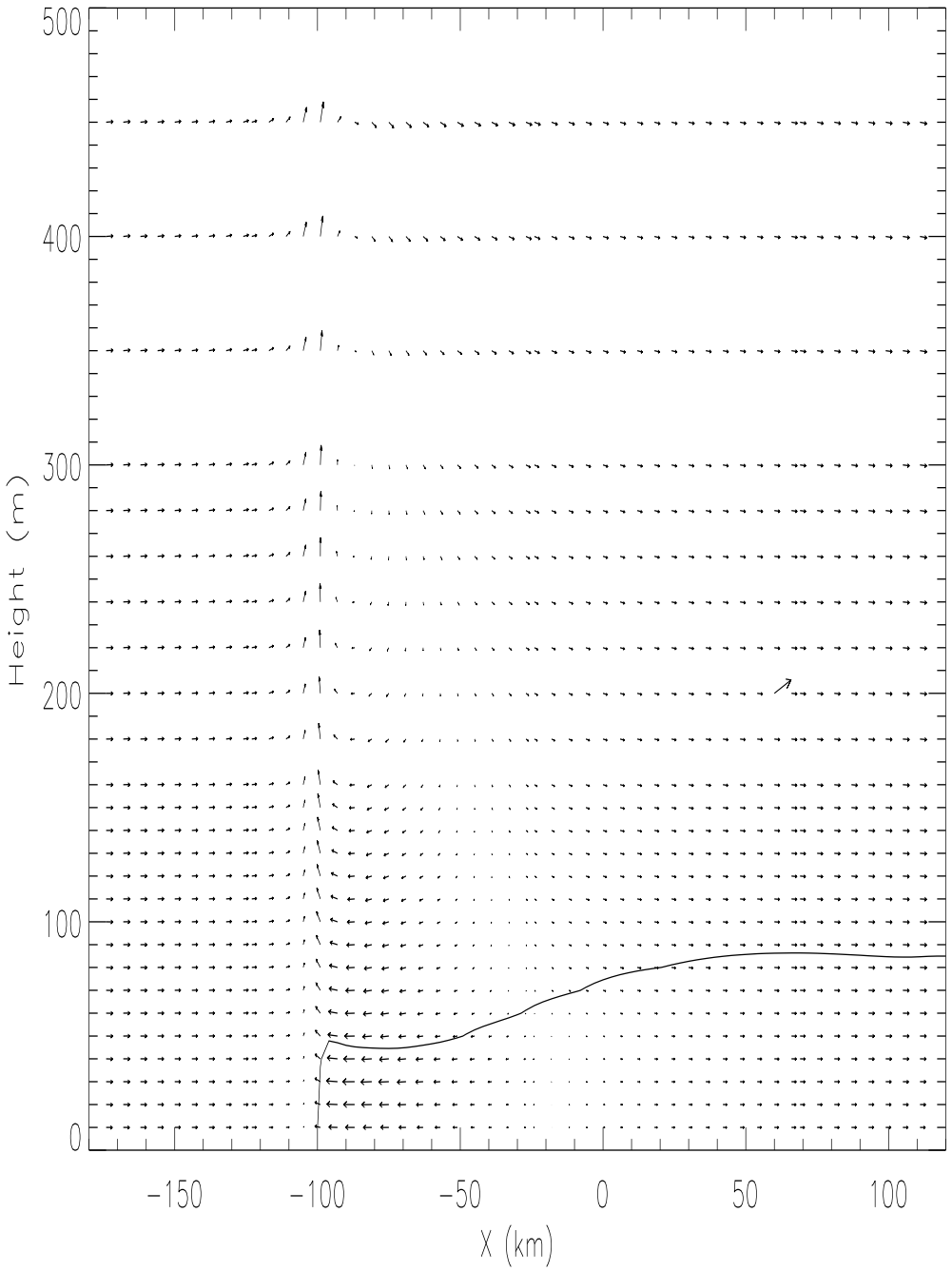

Figure 24: Cross section of the wind at 1500 hr along the line $y = -54$ km in the low wind case. The u component of the wind is plotted in units of ms^{-1} and the w component in units of cms^{-1}. Scales are provided by a reference arrow shown at a height of 200 m and $x \sim 50$ km, representing $u = 20$ ms^{-1} and $w = 20$ cms^{-1}. Also plotted is the contour $q = 12$ mb.

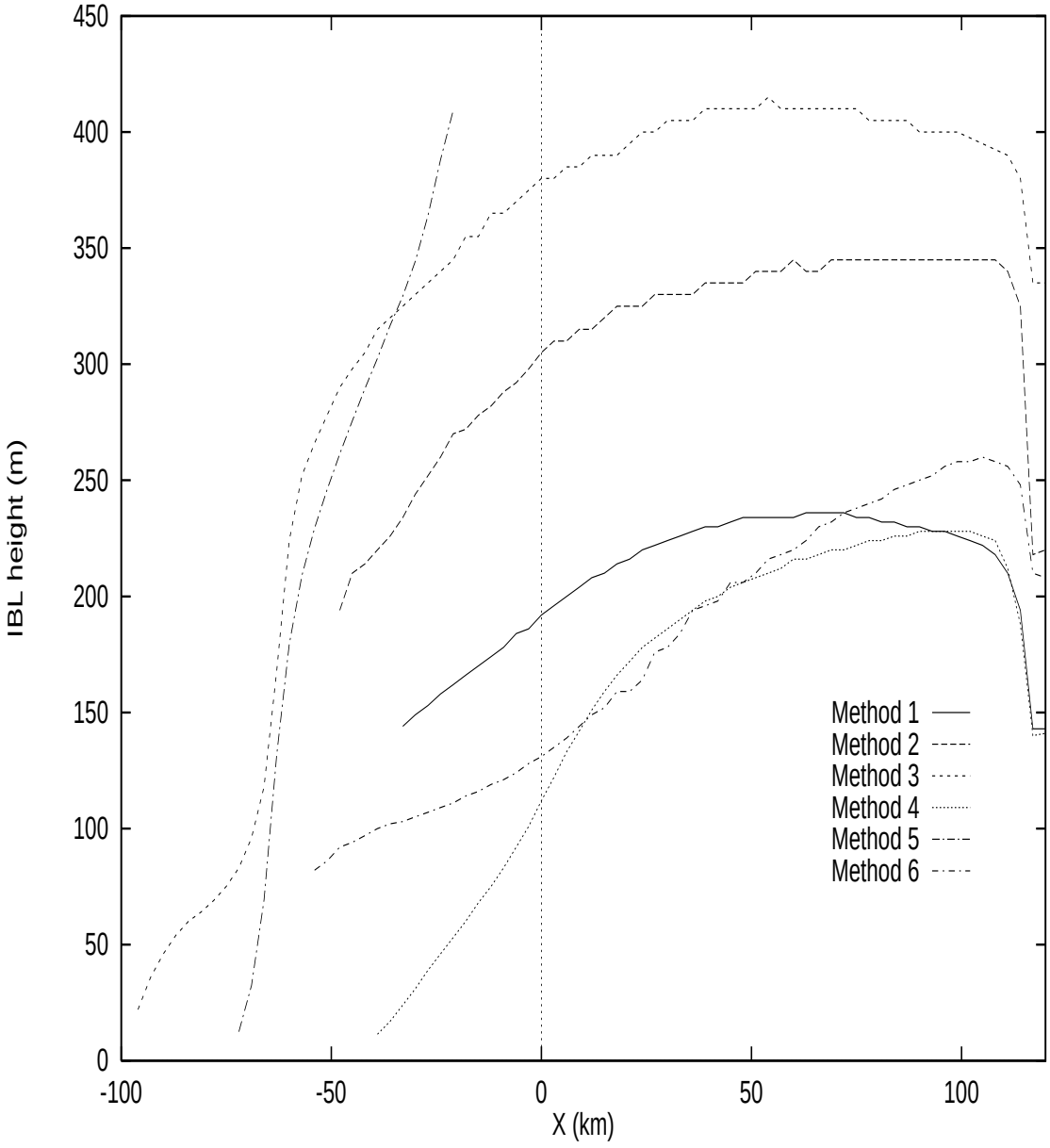

Figure 25: IBL heights according to various methods. The results are plotted as a function of fetch along the line $y = -54$ km at 1500 hr in the high wind case.

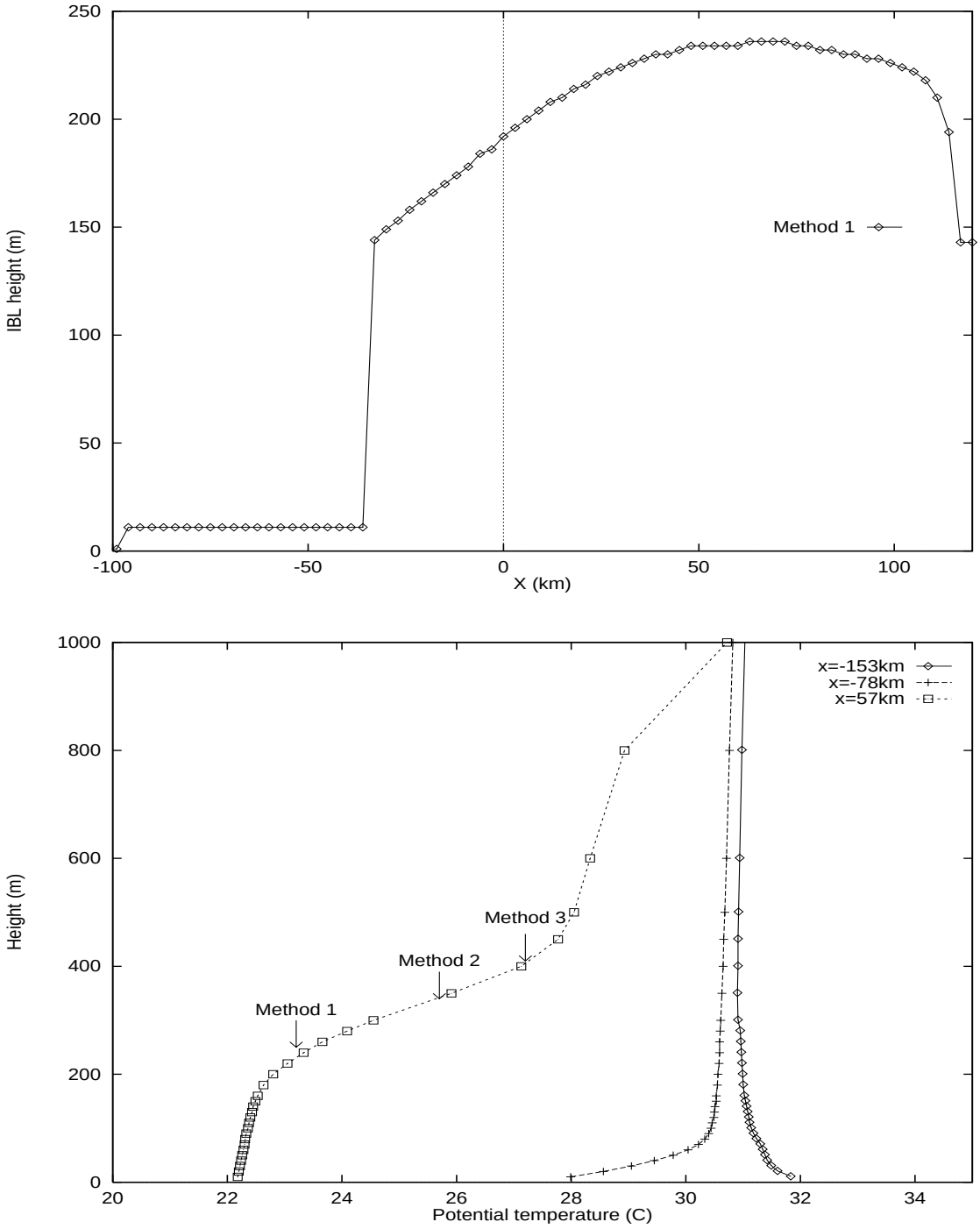

Figure 26: The upper plot shows IBL heights according to method 1. The results are plotted as a function of fetch along the line $y = -54$ km at 1500 hr in the high wind case. The lower plot shows various potential–temperature profiles along this line, also at 1500 hr. Arrows in the lower plot point to IBL heights calculated at $x = 57$ km.

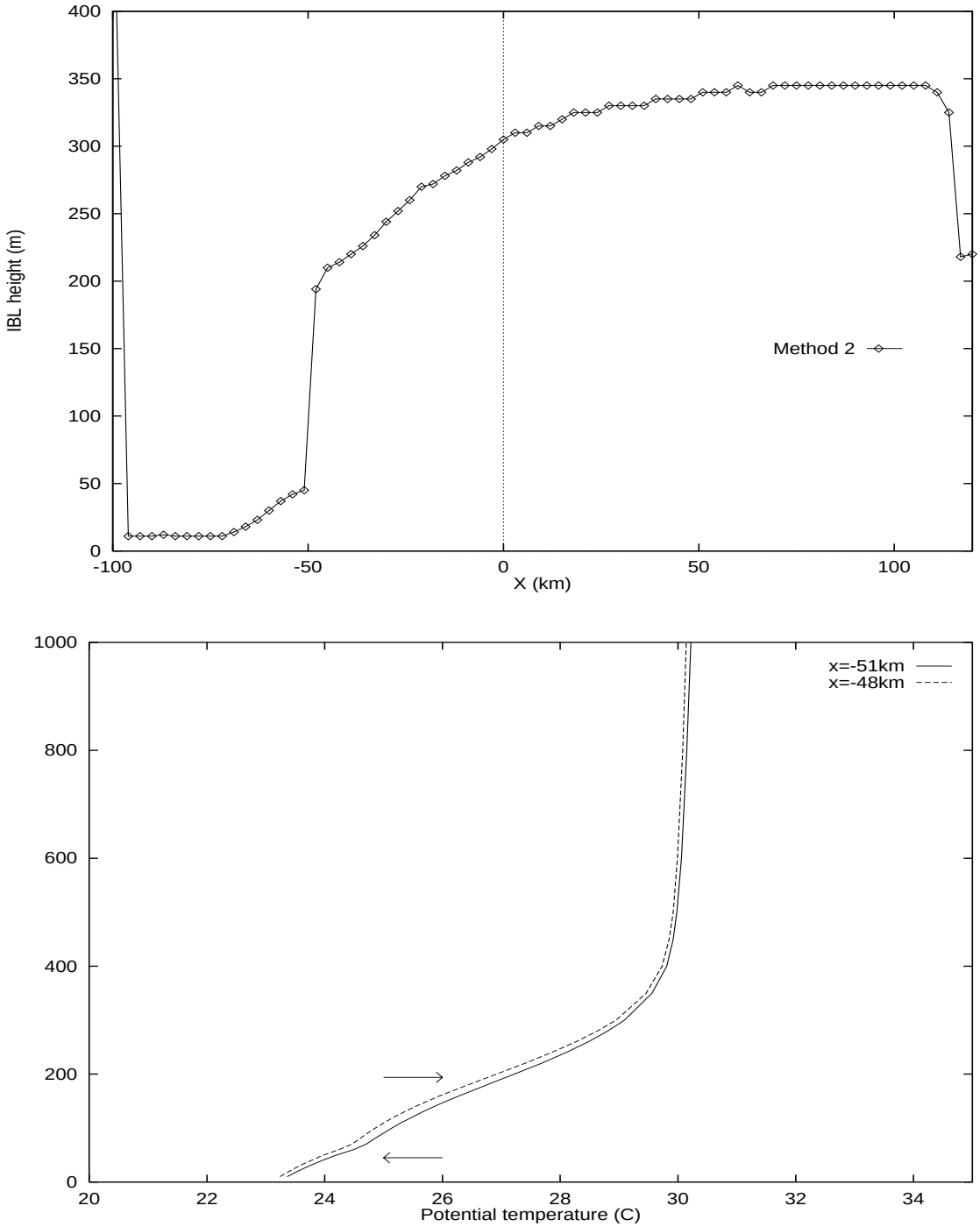

Figure 27: The upper plot shows IBL heights according to method 2. The results are plotted as a function of fetch along the line $y = -54$ km at 1500 hr in the high wind case. The lower plot shows potential–temperature profiles along this line, also at 1500 hr. Arrows in the lower plot point to IBL heights calculated using method 2. The lower arrow marks the height at $x = -51$ km while the upper arrow marks that at $x = -48$ km.

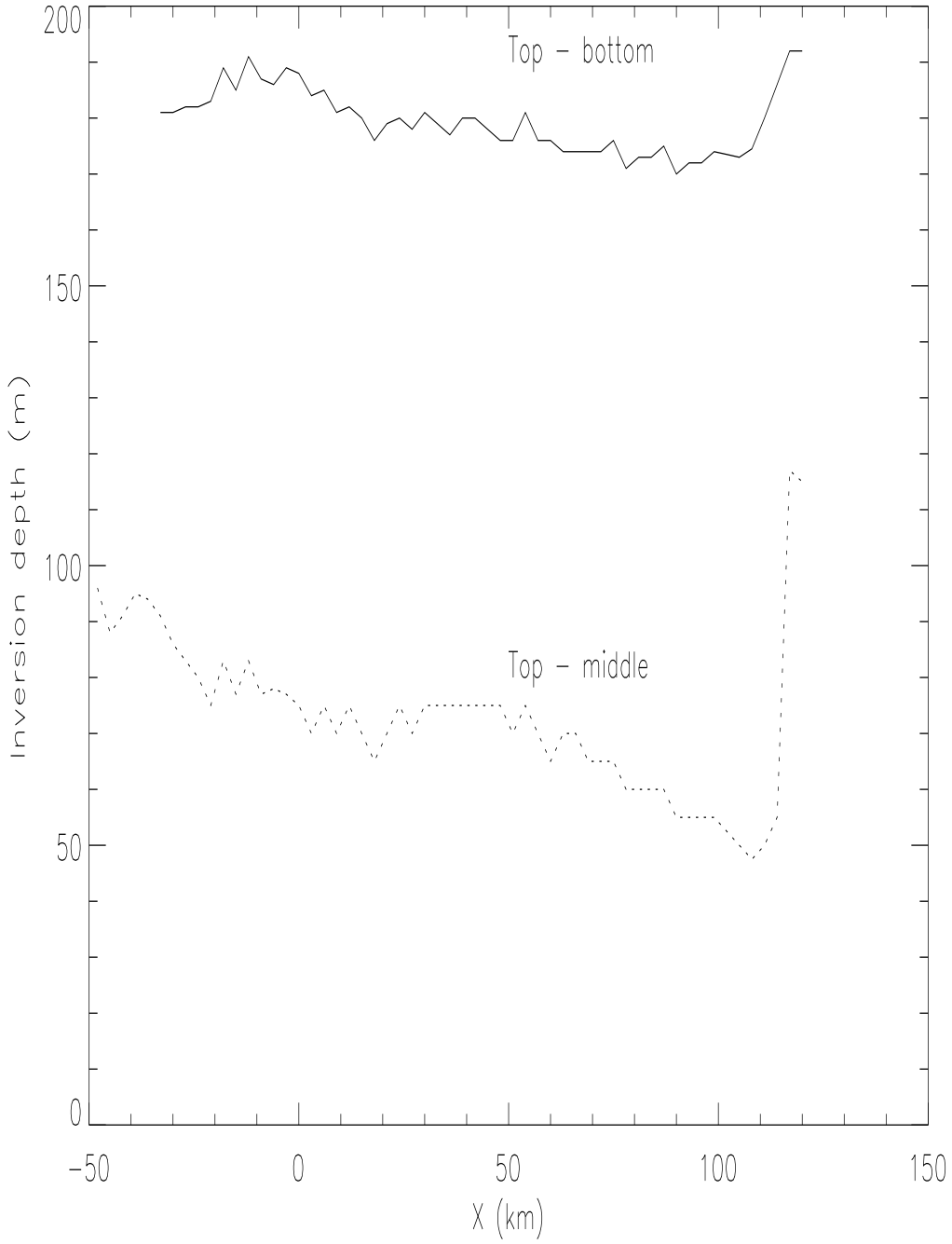

Figure 28: The solid line shows the difference in IBL heights calculated by methods 3 and 1; the dashed line shows the difference in IBL heights calculated by methods 3 and 2. The calculations were performed along the line $y = -54$ km at 1500 hr in the high wind case.

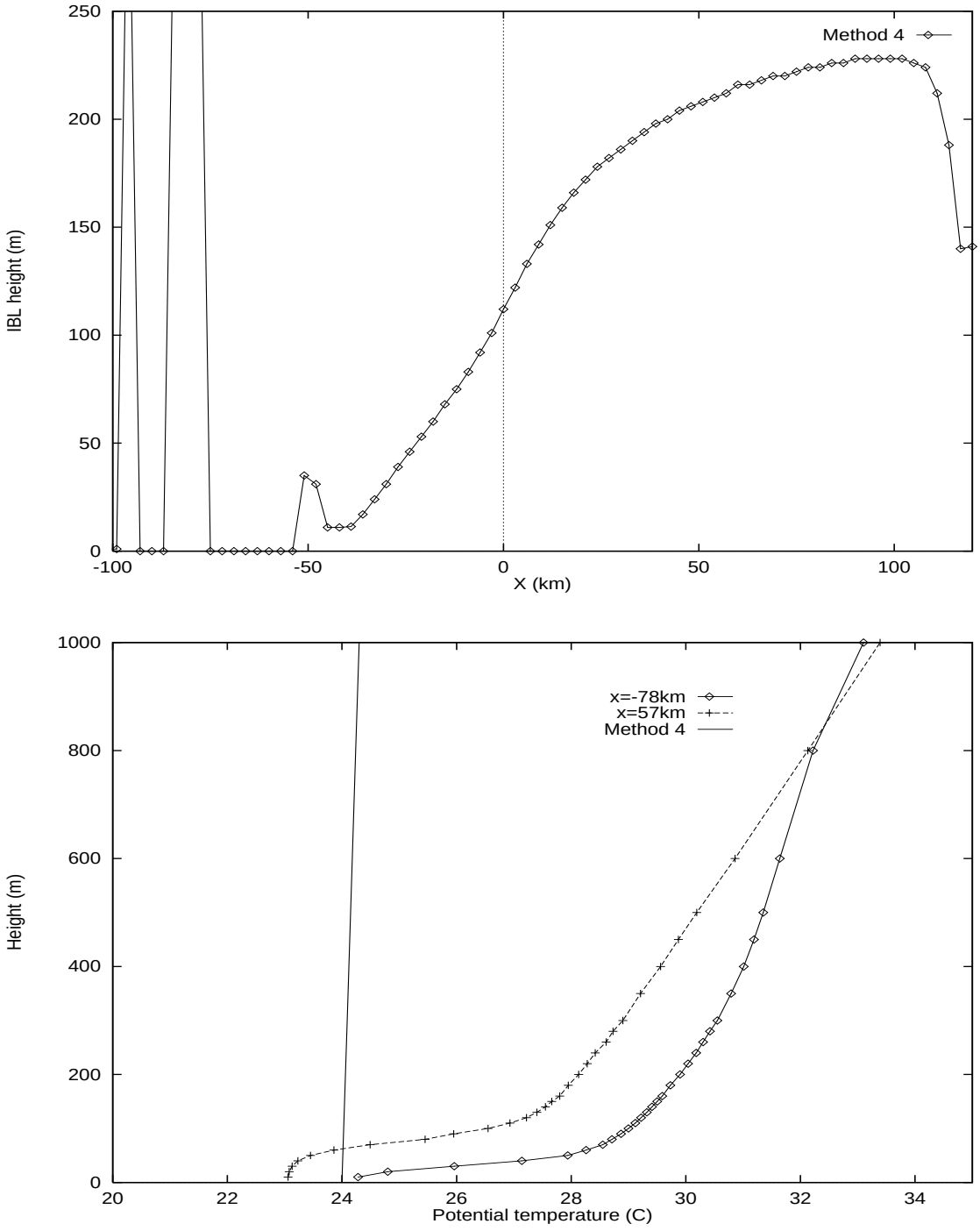

Figure 29: The upper plot shows IBL heights according to method 4. The results are plotted as a function of fetch along the line $y = -54$ km at 1500 hr in the high wind case. The lower plot shows potential–temperature profiles along $y = -54$ km at 1500 hr in the low wind case. Also shown on the lower plot is the reference line used in method 4.

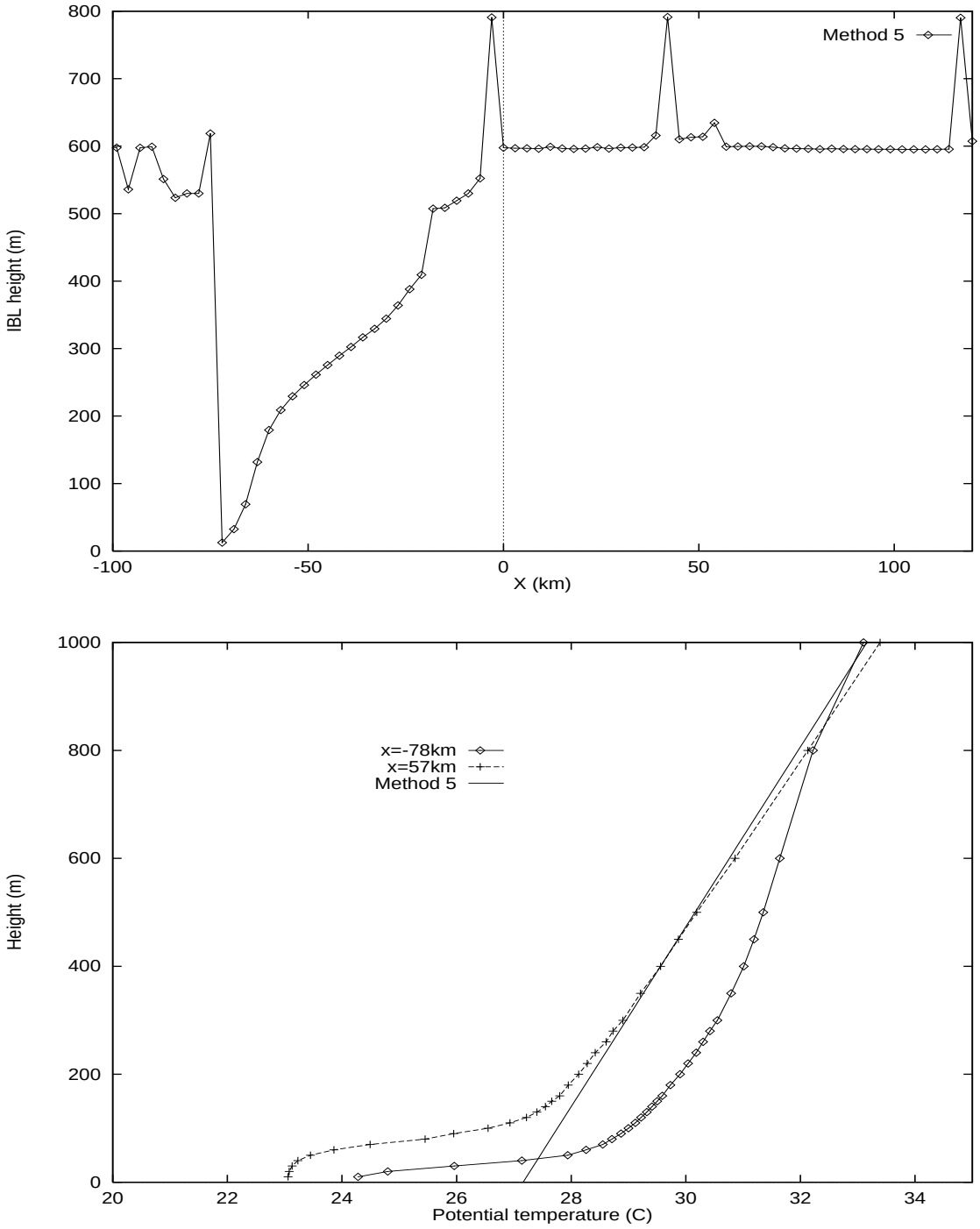

Figure 30: The upper plot shows IBL heights according to method 5. The results are plotted as a function of fetch along the line $y = -54$ km at 1500 hr in the high wind case. The lower plot shows potential–temperature profiles along $y = -54$ km at 1500 hr in the low wind case. Also shown on the lower plot is the reference line used in method 5.

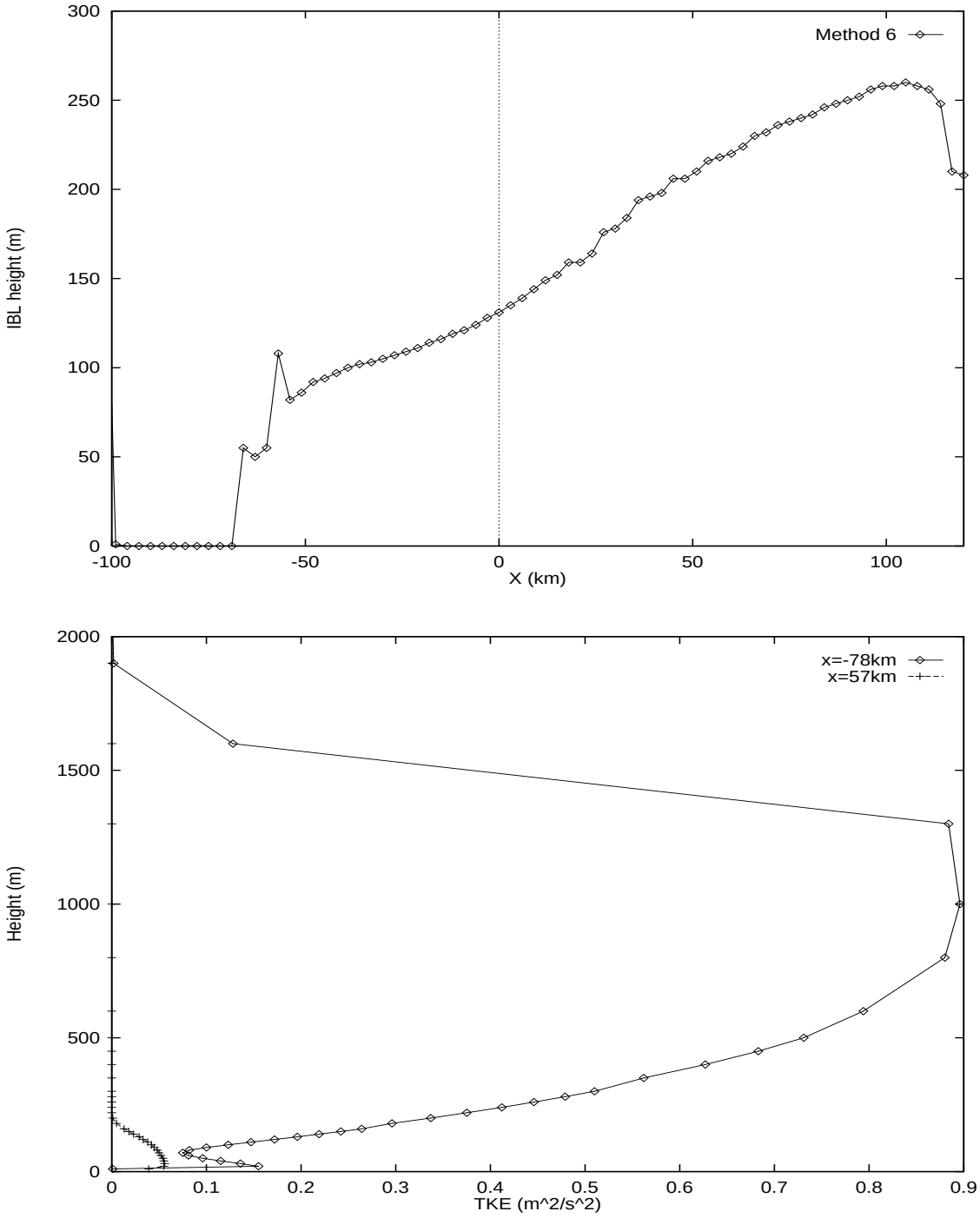

Figure 31: The upper plot shows IBL heights according to method 6. The results are plotted as a function of fetch along the line $y = -54$ km at 1500 hr in the high wind case. The lower plot shows TKE profiles at two points along this line, also at 1500 hr.

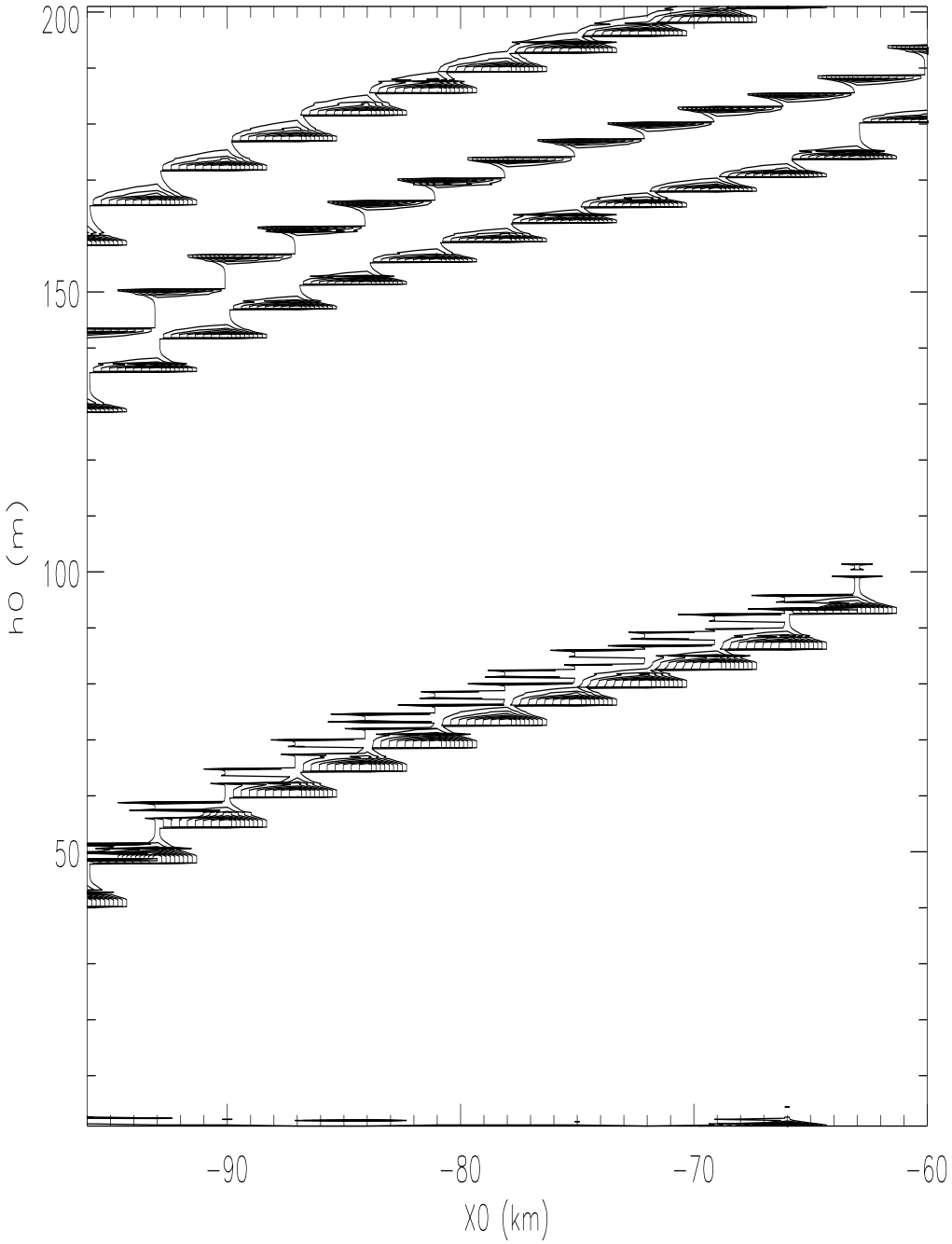

Figure 32: A contour plot of the predicted height of the mature MBL, using the generalized Garratt model. The horizontal axis gives the initial x position, using the co-ordinate of the mesoscale simulation grid. The vertical axis gives the initial MIBL height used. The contours are unlabelled since their only significance lies in the fact that they mark out regions of qualitatively different behaviour (see Appendix B for full details).

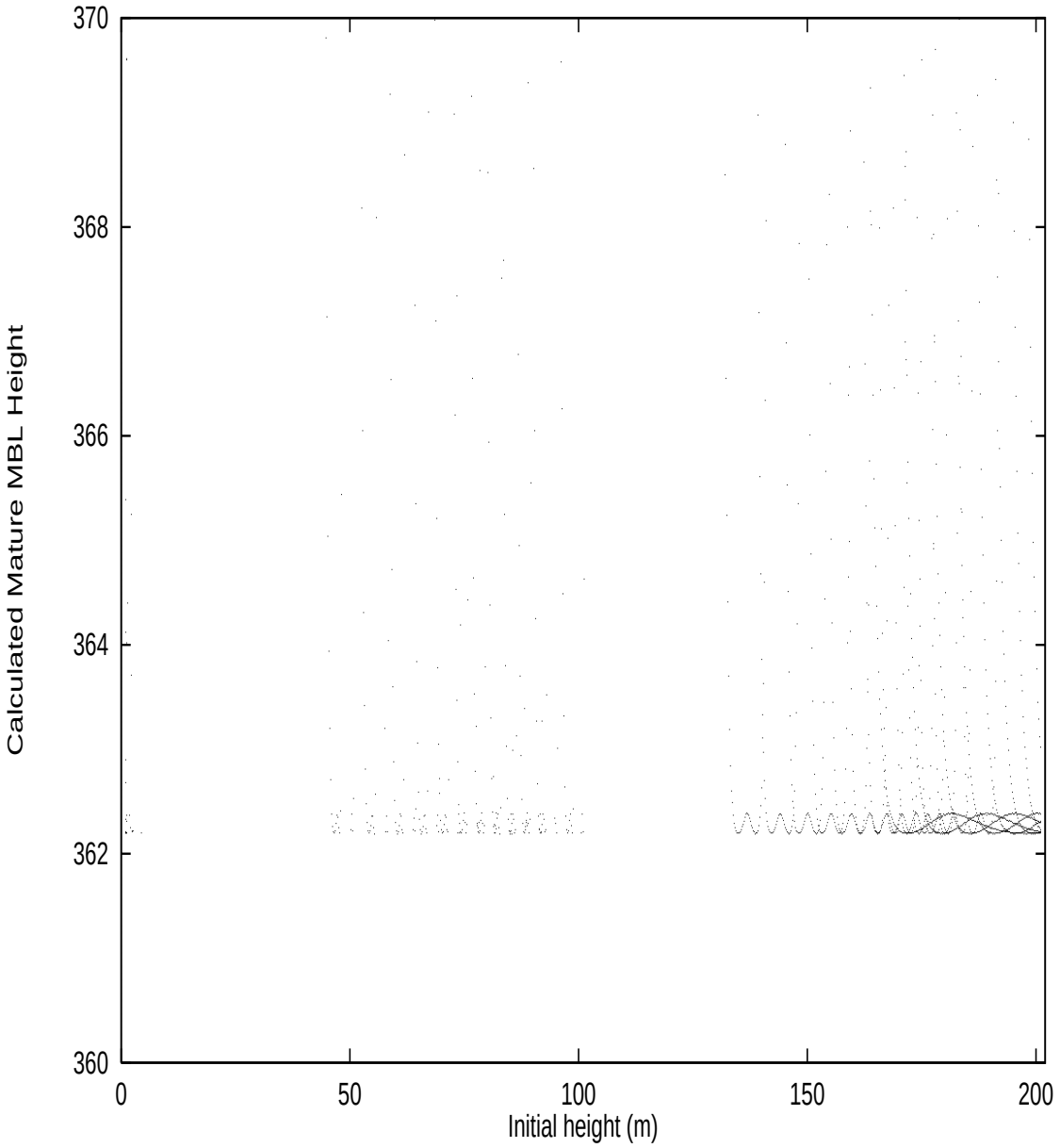

Figure 33: A scatter plot of the predicted height (m) of the mature MBL, using various initial conditions in the generalized Garratt model. The horizontal axis gives the initial MIBL height used.

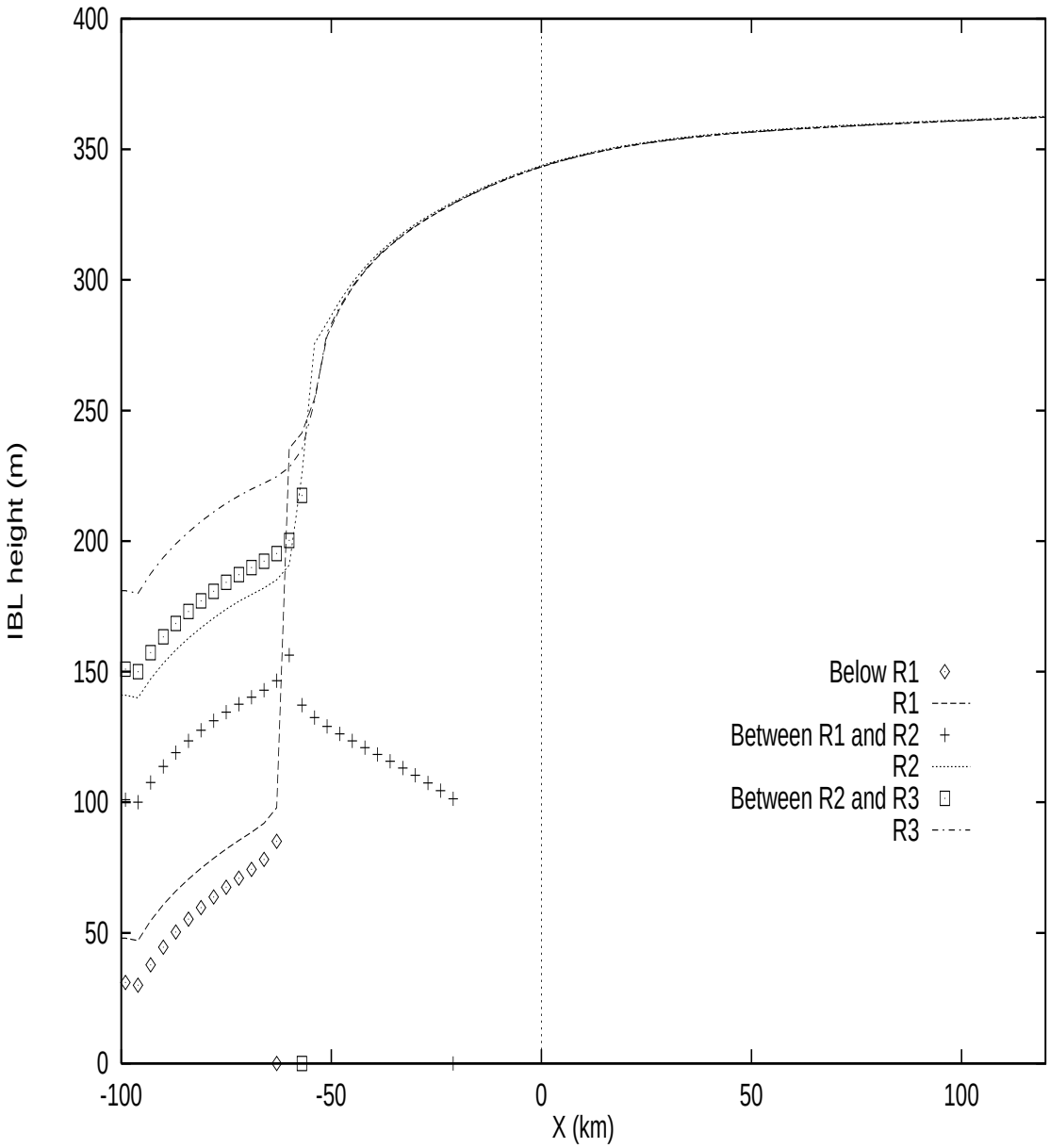

Figure 34: IBL heights predicted from the generalized Garratt model. Each plot corresponds to a different set of initial conditions. Those marked by lines use conditions from within regions 1, 2 and 3. Those marked by points use conditions: below region 1; between regions 1 and 2; and, between regions 2 and 3. The different regions are described in Appendix B.